LAWRENCE
LIVERMORE
NATIONAL
LABORATORY

UCRL-SR-235071

Numerical Modeling of Coupled Groundwater and Surface Water Interactions in an Urban Setting

Jehan F. Rihani, Reed M. Maxwell

September 28, 2007

This work was performed under the auspices of the U.S. Department of Energy by University of California, Lawrence Livermore National Laboratory under Contract W-7405-Eng-48.

Numerical Modeling of Coupled Groundwater and Surface Water Interactions in an Urban Setting

Jehan F. Rihani
Department of Civil and Environmental Engineering
University of California, Berkeley

Reed M. Maxwell
Atmospheric, Earth and Energy Sciences Department
Lawrence Livermore National Laboratory

This work was performed under the auspices of the U.S. Department of Energy by University of California, Lawrence Livermore National Laboratory under Contract W-7405-Eng-48. This work was funded by the FE program of the U. S. Department of Energy.

TABLE OF CONTENTS

Page

LIST OF FIGURES

Page

LIST OF TABLES

Page

1. INTRODUCTION

1.1 The Dominguez Channel Watershed

The Dominguez Channel Watershed (DCW), located in the southern portion of Los Angeles County (Figure A.1), drains about 345 square miles into the Los Angeles Harbor. The cities and jurisdictions in DCW are shown in Figure A.2. The largest of these include the cities of Los Angeles, Carson, and Torrance. This watershed is unique in that 93% of its land area is highly developed (i.e. urbanized). The watershed boundaries are defined by a complex network of storm drains and flood control channels, rather than being defined by natural topography. Table (1) shows a summary of different land uses in the Dominguez Channel Watershed (*MEC, 2004*).

Table (1): Summary of land use within the Dominguez Channel Watershed (*MEC, 2004*).

Land Use	Area (km^2)	Area (mi^2)	Percent of Total
Education	10.5	4.1	3.1
High Density Single Family Residential	100.3	38.7	29.1
Multi-Family Residential	16.6	6.4	4.8
Mixed Residential	12.1	4.7	3.5
Industrial	86.8	33.5	25.2
Retail/Commercial	35.5	13.7	10.3
Transportation	16.7	6.5	4.8
Vacant	34.1	13.2	9.9
Harbor Waters	32.9	12.7	9.5
TOTAL	345	133	100

The Dominguez Watershed has the highest impervious area of all watersheds in the Los Angeles region. The more impervious the surface, the more runoff is generated during a storm. Storm water runoff can carry previously accumulated contaminants and transport them into receiving water systems. Point sources such as industrial wastewater and municipal sewage as well as urban runoff from commercial, residential, and industrial areas are all recognized as contributors to water quality degradation at DWC.

Section 303(d) of the 1972 Federal Clean Water Act (CWA) requires states to identify and report all waters not meeting water quality standards and to develop action plans to pursue the water quality objectives. These plans specify the maximum amount of a given pollutant that the water body of concern can receive and still meet water quality standards. Such plans are called Total Maximum Daily Loads (TMDLs). TMDLs also specify allocations of pollutant loadings to point and non-point sources taking into account natural background pollutant levels. This demonstrates the importance of utilizing scientific tools, such as flow and transport models, to identify contaminant sources, understand integrated flow paths, and assess the effectiveness of water quality management strategies.

Since overland flow is a very important component of the water balance and hydrology of DCW, a parallel, distributed watershed model that treats flow in groundwater and surface water in a dynamically coupled manner will be used to build a flow model of the watershed. This coupled model forms the basis for modeling and understanding the transport of contaminants through the Dominguez Channel Watershed, which can be used in designing and implementing TMDLs to manage the water quality in this basin.

In this report, the coupled surface water-groundwater flow model of DCW will be presented. This flow model was calibrated against a storm that occurred in February 21st, 2004. The model and approach are explained further in the following sections.

2. Computer Code and Governing Equations

To better simulate the interactions between surface water and groundwater at DCW, the parallel three dimensional variably saturated subsurface flow code Parflow (*Ashby and Falgout, 1996; Jones and Woodward, 2001*), coupled to a new two-dimensional overland flow simulator (*Kollet and Maxwell, 2006*), was used in modeling this watershed. This new coupled approach does not rely on the conductance concept (e.g. *Anderson and Woessner, 1992*) usually utilized in such applications. Instead, it directly couples the surface and subsurface systems via a boundary condition applied at the ground surface.

The system of equations being coupled in this new formulation is briefly described in Section 2.1, which shows how Parflow utilizes conditions of pressure and flux continuity at the ground surface to implement the overland flow equations into the Richard's equation when the upper boundary cell becomes saturated. For complete details, the reader is referred to Kollet and Maxwell (2006).

2.1. Governing Equations

2.1.1 Shallow overland flow equations:

The Continuity equation can be written as follows for a two dimensional problem (*Kollet and Maxwell, 2006*):

$$\frac{\partial \psi_s}{\partial t} = \nabla \vec{v} \psi_s + q_r(x) \qquad \text{(Equation 1)}$$

Where; v is the depth averaged velocity vector [L/T], ψ_s is the surface ponding depth [L], $q_r(x)$ is the general source/sink rate [L/T]. This formulation neglects the vertical change in momentum since the flow depth is vertically averaged. When diffusion terms are neglected, the momentum equation simplifies to the kinematic wave approximation (*Kollet and Maxwell, 2006*):

$$S_{f,i} = S_{o,i} \qquad \text{(Equation 2)}$$

Where; $S_{f,i}$ is the friction slope in the x or y direction [L], $S_{o,i}$ is the bed slope or gravity forcing term [-], and *i* stands for the x and y directions. Manning's equation is used to obtain a flow depth – discharge relationship (*Kollet and Maxwell, 2006*):

$$v_x = \frac{\sqrt{S_{f,x}}}{n}\psi_s^{2/3} \qquad and \qquad v_y = \frac{\sqrt{S_{f,y}}}{n}\psi_s^{2/3} \qquad \text{(Equation 3)}$$

Where; *n* is Manning's friction coefficient [$T/L^{1/3}$].

2.1.2 Variably saturated GW flow:

Richard's equation is used to model variably saturated groundwater flow (Jones and Woodward, 2001; *Kollet and Maxwell, 2006*):

$$S_s S_w \frac{\partial \psi_p}{\partial t} + \phi \frac{\partial S_w(\psi_p)}{\partial t} = \nabla . q + q_s$$

(Equation 4)

$$q = -k(x)k_r(\psi_p)\nabla(\psi_p - z)$$

Table (2): Model Domain and Grid.

	Model Coordinates		
	X (m)	Y (m)	Z (m)
Upper x, y, or z	23,939.8	17,721.7	2.0
Lower x, y, or z	0	0	0
dx, dy, or dz (m)	310.907	310.907	0.1
nx, ny, or nz	57	77	20

Where; *z* is depth below the surface [L], ψ_p is the subsurface pressure head [L], *k(x)* is the saturated hydraulic conductivity [L/T], *kr* is the relative permeability [-], S_s is the specific storage coefficient [L^{-1}], ϕ is the porosity [-], S_w is the Degree of saturation [-], and q_s is the general source/sink term [T^{-1}]

2.1.3 Boundary Condition at the Land Surface

Continuity of pressure ($\psi_p = \psi_s = \psi$) and flux ($q_{bc}=q_e$) at the ground surface gives the boundary condition at the land surface (*Kollet and Maxwell, 2006*):

$$-k(x)k_r\nabla(\psi - z) = \frac{\partial \|\psi.0\|}{\partial t} - \nabla\vec{v}\|\psi.0\| - q_r(x) \qquad \text{(Equation 5)}$$

3. Watershed Discretization and Model Design

3.1 Model and Grid Design

The Dominguez Channel watershed was simulated within a box-shaped domain with dimensions of about 17.7 km by 23.9 km by 2 m in the x-, y-, and z-directions, respectively

(Table 2). Figure (1) shows the conceptual model of DCW. The black area around the watershed in figure (1) consists of inactive cells. No flow or pressure is calculated within these cells. Simulation only takes place in the active cell region within the watershed boundaries shown in the same figure.

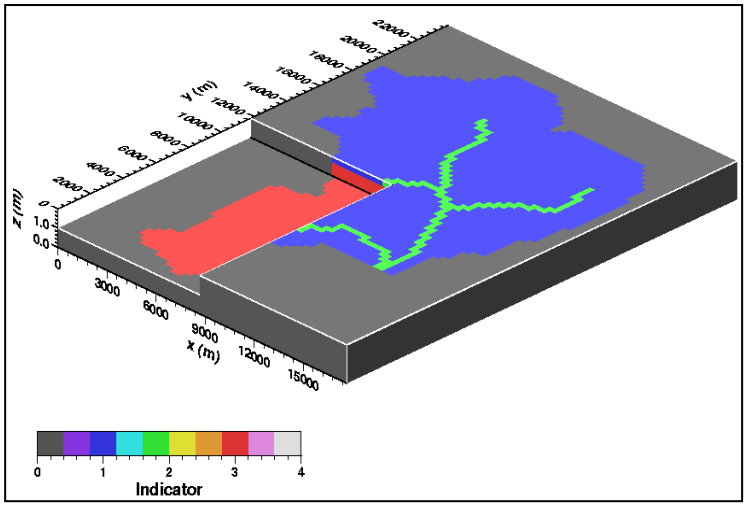

Figure (1): Conceptual model of Dominguez Channel watershed.

The top three layers of the active domain represent the urbanized land surface and the Dominguez channel. Active cells beneath those surface layers were assigned as the subsurface beneath DCW. Thus, three different sets of land/soil properties where introduced into the model and calibration process. This was introduced by means of an indicator field, which can be used in the same way to introduce more different land use types to the surface and more heterogeneity in the subsurface, if required.

3.2 Model Parameters

Based on the conceptual model and formulation described previously, the model parameters assigned are; hydraulic conductivities and porosities for field, channel, and subsurface, Manning's coefficients for the field and channel, specific storage, relative permeability parameters, and surface slopes. The slopes were calculated (as x- and y-slopes) based on the DCW digital elevation model (Figure 2). To prevent numerical instabilities, these slopes were processed to eliminate sinks in the surface. Figure 3 shows the resulting processed slope vectors used in the model enlarged 10 times. Finally, the Van Genuchten equations (Van Genuchten, 1980) were used to describe the relative saturation and permeability.

This formulation allows for the urbanization of the surface to be taken into account, by assigning low hydraulic conductivity and porosity for the field and even lower values to the concrete channel, while still being able to assign reasonable subsurface parameters to allow for infiltration and water table fluctuations.

3.3 Sources, Sinks and Simulation Time

The model was calibrated against observed outflow in the DCW resulting from a storm event that occurred on February, 21st 2004. Time variable rainfall radar data was obtained from the National Oceanic and Atmospheric Administration's (NOAA) National Weather Service (NWS) using the Stage III assimilated precipitation product. Furthermore, the watershed has three rainfall gages within its boundaries; One at Los Angeles International Airport (LAX), one

within the center of the watershed, and one at the outlet (Figure A.3). Since the radar data is averaged over the entire watershed area, once the model was calibrated it was run using the each of the three rain gage data to verify that the model behavior envelopes the spatial variability in rainfall. Figure (4) shows the radar rainfall data as well as the rain gage data. The recorded hydrograph of that storm is also shown in the figure. No evaporation was assumed during the storm simulation. Also, based on the Feb 21st storm, the simulations were set to 27 hours with 5 minute time steps.

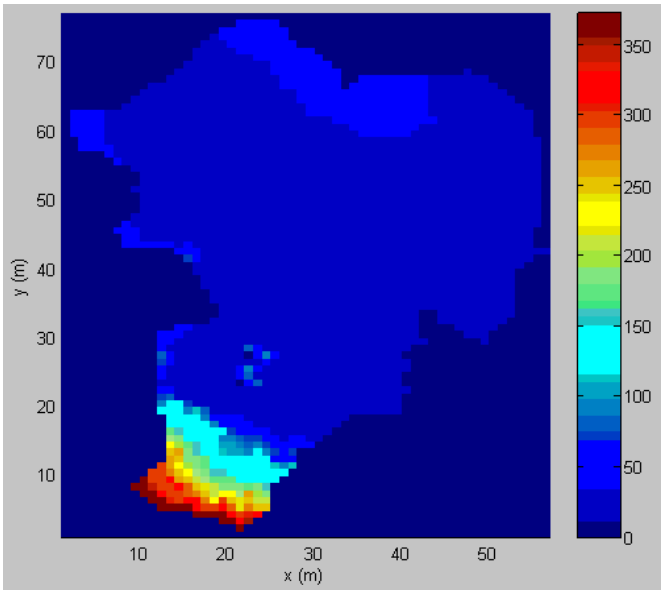

Figure (2a): Digital elevation model for the Dominguez channel watershed.

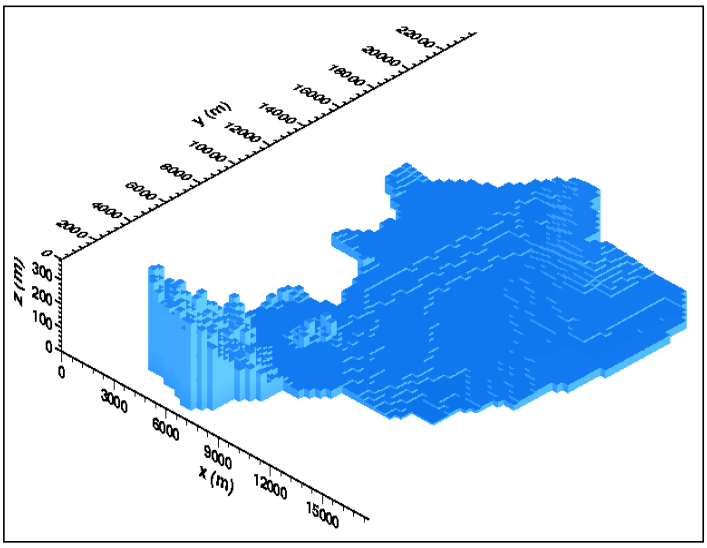

Figure (2b): Digital elevation model (converted to a three-dimensional solid file)

3.4 Initial and Boundary Conditions

Nuemann-type boundary conditions are applied for the DCW model. For the perimeter and bottom boundary, no flow conditions were applied. The overland flow boundary condition was applied at the top layer. As for initial conditions, the water table was assigned at the bottom layer of the domain at the beginning of the simulation.

4. Flow Model Calibration and Parameter Sensitivities

The model was calibrated under transient conditions against the radar rainfall data for the Feb. 21st storm. Table B.1 shows a record of the calibration runs in which the model parameters were modified in order to match the observed hydrograph. The table also shows a calculation of the watershed mass balance for each run. The mass balance components, computed as volume in m^3, are as follows; Total precipitation (P), total overland flow or runoff (Q), compressible subsurface storage (Sc), pore storage (Sp), and surface storage (Ss). The mass balance is calculated as follow:

$P - Q = \text{Total Storage } (Sc+Sp+Ss) \rightarrow P - Q - Sc - Sp - Ss = \text{Error}$ (Equation 6)

Table 3 summarizes the runs used to test the model's sensitivity to certain calibration parameters while Figures B.1 through B.10 show the corresponding effects in the simulated hydrograph. During runs without a subsurface layer assigned, the domain would saturate quickly, because of the very low porosity and hydraulic conductivity used to match the urbanization of the surface. This clearly affected the behavior of the simulated hydrograph at later times in the simulation (Figure B.1) because the total volume of outflow was overestimated as the water could not infiltrate into the already saturated domain. Once the subsurface was added and lower porosity and hydraulic conductivity were assigned beneath the surface layer(s), the model responded more readily to changes in field and channel parameters. The vertical grid size had a similar effect (Figure B.2) since smaller grid cells saturate faster. Figure B.2 shows the rising tail of the simulated hydrograph for run35 which has a grid size of 0.1 meters in the vertical. Run34, which has twice that vertical grid size, does not show this effect.

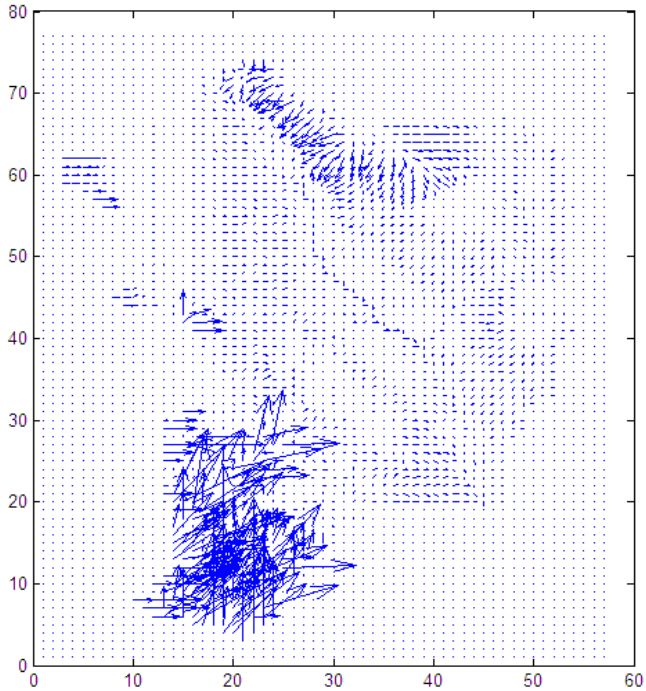

Figure (3): Processed slope vectors calculated from the Dominguez Channel watershed digital elevation model.

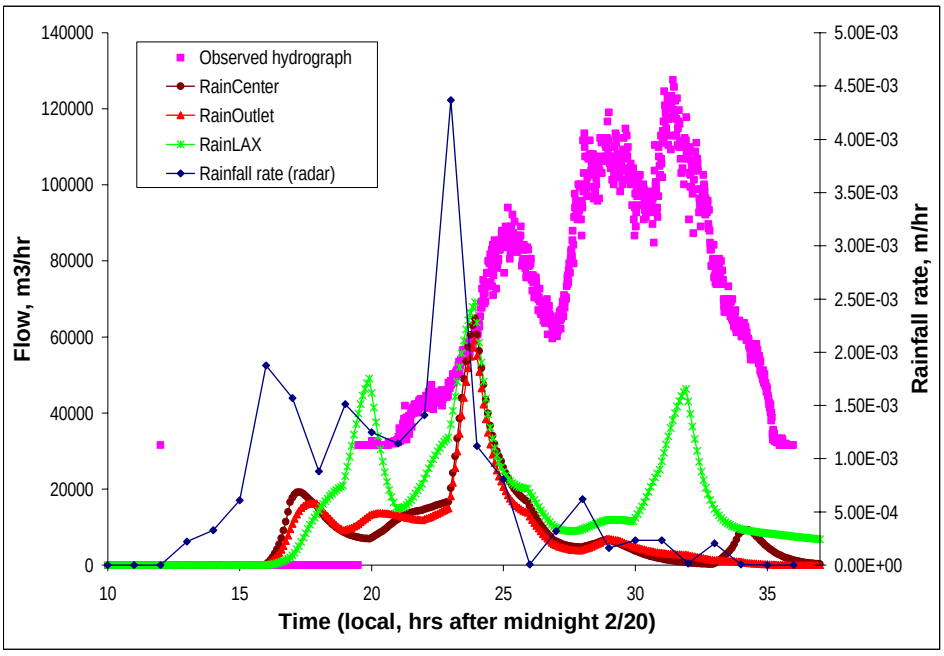

Figure (4): Radar and rain gage storm data along with the resulting observed hydrograph at DCW.

Table (3): Summary of parameter sensitivity runs with reference to corresponding figures in Appendix B.

Parameter	Runs compared			Figure
	Run number (parameter value)			
Subsurface added	run21 (without subsurface)	run49 (with subsurface)	(-)	B.1
Vertical grid size, dz (m)	run35 (0.1)	run34 (0.2)	(-)	B.2
Channel Manning ($hr/m^{1/3}$)	run70 (1.0E-7)	run72 (2.0E-7)	run71 (3.0E-7)	B.3
Field Manning ($hr/m^{1/3}$)	run51 (1.0E-6)	run52 (5.0E-6)	run49 (2.0E-5)	B.4
Channel porosity	run70 (0.00009)	run69 (0.0001)	(-)	B.5
Field porosity	run30 (0.001)	run31 (0.01)	(-)	B.6
Subsurface porosity	run57 (0.01)	run59 (0.2)	(-)	B.7
Field hydraulic conductivity (m/hr)	run55 (0.0005)	run54 (0.001)	run53 (0.003)	B.8
Thickness of field layer	run54 (1 layer)	run57 (2 layers)	run65 (3 layers)	B.9
Field slopes	run37 (0.5*field slopes)	run45 (0.25*field slopes)	run46 (0.05*field slopes)	B.10

Changes in the field Manning's coefficient had a greater effect on the hydrograph and total runoff volume than changes in the channel Manning's coefficient as shown in figures B.3 and B.4. This is true, despite the fact that the range of variability in the channel Manning's coefficient was smaller than that for the field. It follows that the field friction has a higher effect on the total outflow as there are more cells assigned as field cells than assigned as channel cells. Thus, a much larger amount of rainfall runoff is affected by the field Manning's than the channel.

Not much sensitivity was observed in the case of the channel porosity, since this is originally assigned at a very low value (Figure B.5). Higher effects are noticed for changing the field and subsurface porosities as shown in figures B.6 and B.7. Furthermore, since the field hydraulic conductivity was assigned to low values due to the urbanization of the DCW, changing it had little effect on the hydrograph (Figure B.8).

One important factor in the model design was selecting the appropriate number of layers on the top of the domain to be assigned to the field and channel. These top layers would directly affect the process of runoff generation in the model since the top cells need to saturate before this occurs, and this process in turn is related to the rate of infiltration to the subsurface. This rate of infiltration depends on the vertical effective hydraulic conductivity. As more layers are assigned to the field, the vertical effective hydraulic conductivity becomes less and thus more surface runoff is generated. This effect is shown in Figure B.9 which shows that the total runoff volume is inversely related to the number of the field assigned layers.

Finally the sensitivity of the model to changing thye processed field slopes (from figure 3) is shown in Figure B.10 which shows a direct relationship between this and the total runoff volume. This is not unexpected since smaller slopes give the ponded water on the surface more time to infiltrate into the subsurface.

5. Results

Table 4 shows the model parameters of the calibrated simulation run (run72). The hydraulic conductivity and porosity fields for this run are shown in Figures 5 and 6, respectively. This run has the three top layers assigned for the field and channel with much lower hydraulic conductivities and porosities than the subsurface. The total runoff volume was about 29% of the total precipitation volume.

Table (4): Summary of calibrated run parameters.

RUN NAME	run72
Vertical Grid Size	**dz = 0.1, 3 cell field**
Specific Storage	**Ss=1.0E-4**
Change in Slopes	**Half field slopes**
Channel Ksat (m/hr)	**K_chann=0.0001**
Field Ksat (m/hr)	**K_field=0.001**
Subsurface Ksat (m/hr)	**K_subsurf=0.05**
Channel Porosity	**por_chann=0.00009**
Field Porosity	**por_field=0.003**
Subsurface Porosity	**por_subsurf=0.01**
Channel Manning's Coefficient ($hr/m^{1/3}$)	**n_chann=2.0E-7**
Field Manning's Coefficient ($hr/m^{1/3}$)	**n_field=6.0E-6**
Precipitation (P)	4.229E+06
Runoff (Q)	1.241E+06
Compressible Storage (Sc)	3.967E+04
Pore Storage (Sp)	2.174E+06
Total (Sp+Sc)	2.214E+06
Surface Storage (ponding) (Ss)	7.344E+05
Error (P-Q-Ss-Sp-Sc)	**3.994E+04**
Error (percent of P)	0.9444
Q / P (%)	**29.3379**

Since the radar rainfall data was used in calibrating the model, the effect of rainfall spatial variability was tested by running this simulation (run 72) for the same storm event but with the rainfall data recorded at each of the three rainfall locations within DCW (at LAX, center, and outlet of the domain). Figure 7 shows the calibrated hydrograph for run72 (with radar rainfall data averaged over the domain), and the resulting hydrographs for the three individual rainfall rain gage data locations. These hydrographs provide an envelope of prediction that encompasses both the observed outflow and the simulation using the averaged rainfall observations. This demonstrates that the spacial variability in rainfall at locations around the DWC is greater than differences between calibration runs.

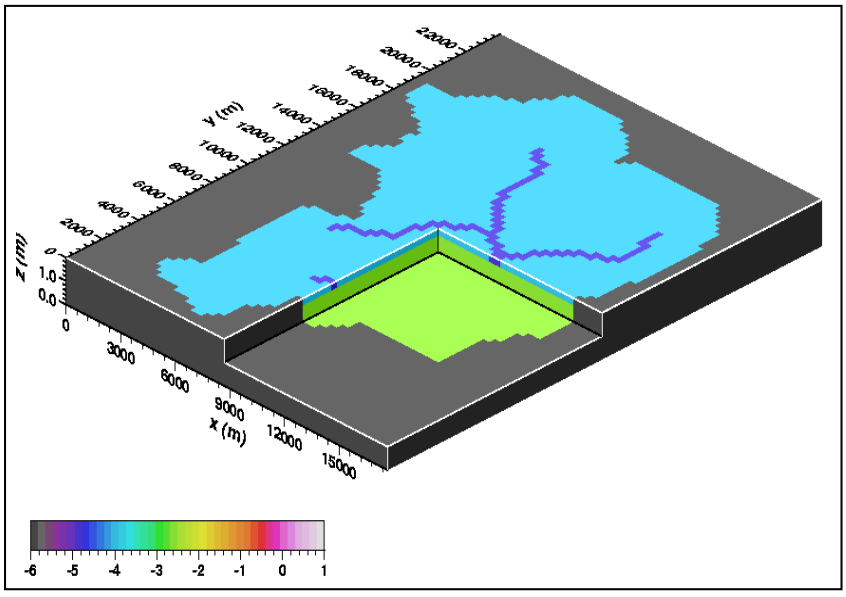

Figure (5): Calibrated Saturated Hydraulic Conductivity Field in m/hr (log scale) of Dominguez Channel watershed.

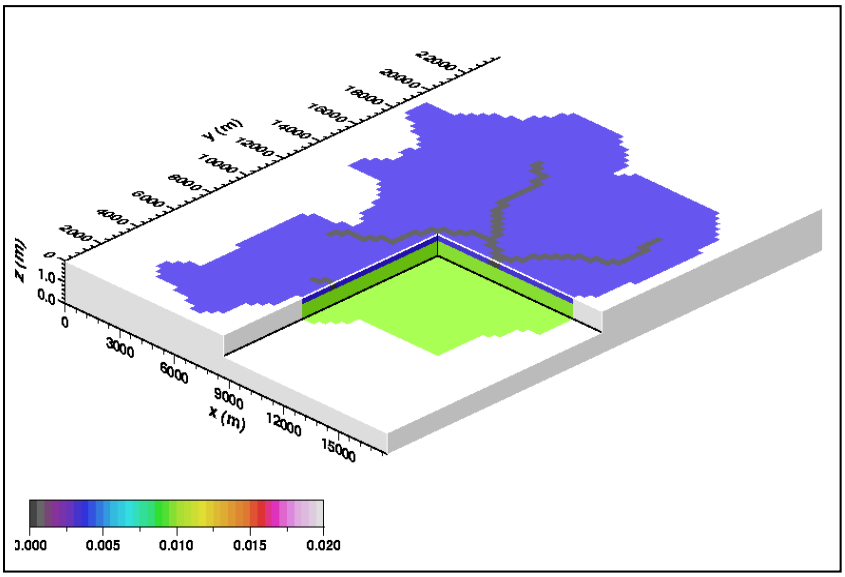

Figure (6): Calibrated Porosity Field of Dominguez Channel watershed

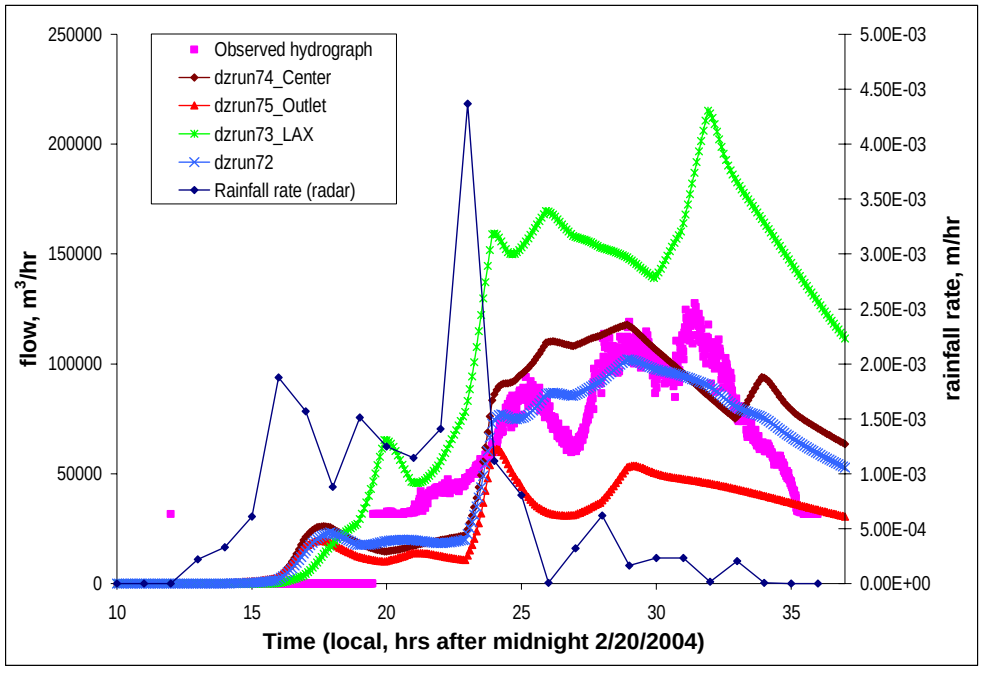

Figure (7): The calibrated hydrograph (run72) and runs with rain gage rainfall data for the same storm.

6. References:

Anderson MP, Woessner WW (1992). “Applied groundwater modeling: Simulation of flow and advective transport”. San Diego: Academic Press, p. 281.

Ashby, S.F. and R.D. Falgout (1996). A parallel multigrid preconditioned conjugate gradient algorithm for groundwater flow simulations. Nuclear Science and Engineering, 124(1):145-59..

Jones J.E. and C.S. Woodward (2001), Newton-krylov-multigrid solvers for large-scale, highly heterogeneous, variably saturated flow problems. Advances in Water Resources, 24:763-774.

Kollet S.J. and RM Maxwell (2006) Integrated surface-groundwater flow modeling a free-surface overland flow boundary condition in a parallel groundwater flow model. Advances in Water Resources, 29(7): 945-958.

MEC Analytical Systems, Inc. (MEC). April 2004. Dominguez Watershed Management Master Plan, “An urban industrial watershed in balance with the environment”. Prepared for the Dominguez Watershed Advisory Council, County of Los Angeles Department of Public Works,

National Oceanic and Atmospheric Administration's National Weather Service (NWS); NEXRAD Rainfall Radar data (http://dipper.nws.noaa.gov/hdsb/data/nexrad/nexrad.html).

Van Genuchten M. Th., (1980), “A closed-form equation for predicting the hydraulic conductivity of unsaturated soils”. Soil Science Society of America Journal, 44:892–898.

APPENDIX A: Dominguez Channel Watershed

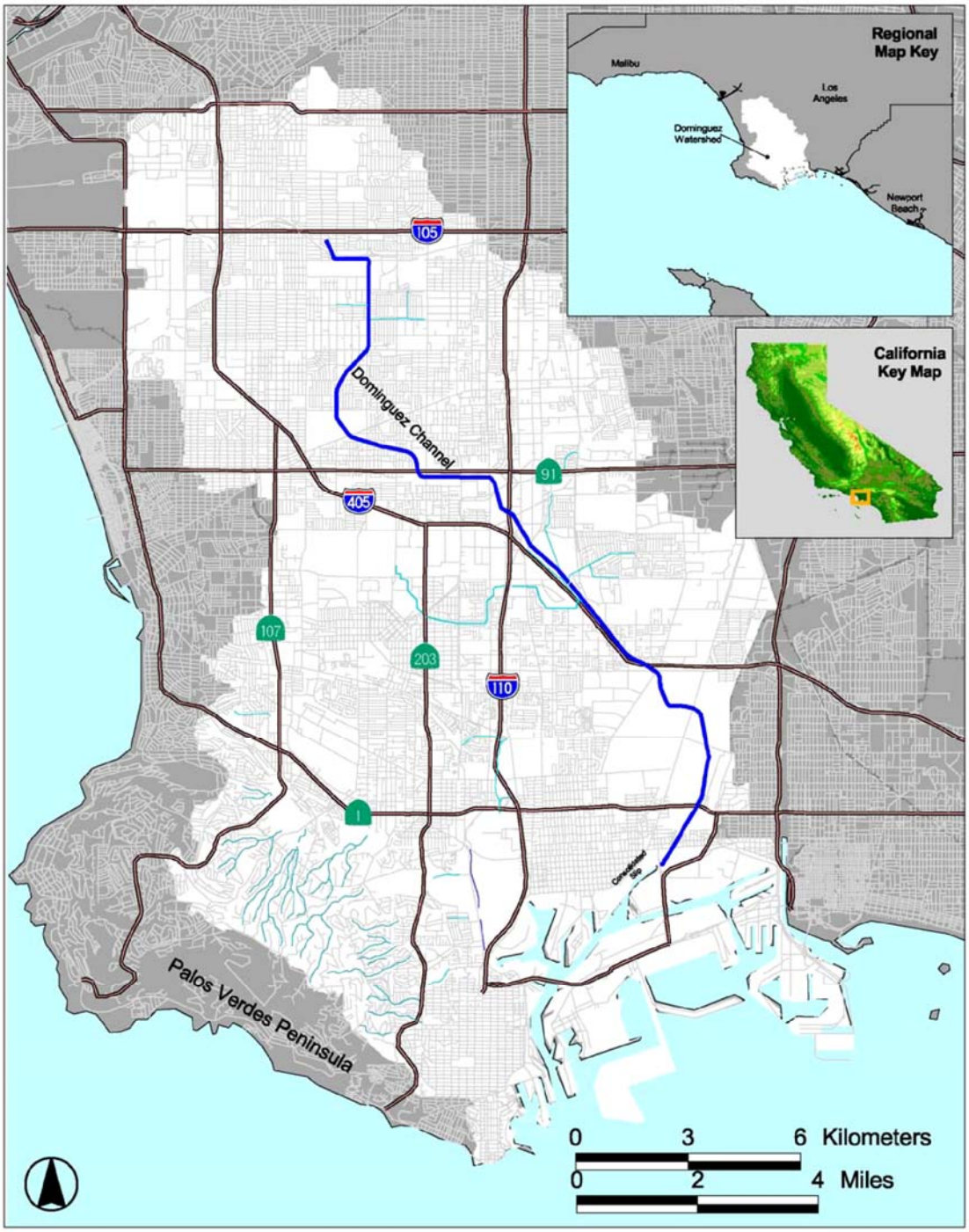

Figure A.1: Regional map showing the location of the Dominguez Channel Watershed (*MEC, 2004*).

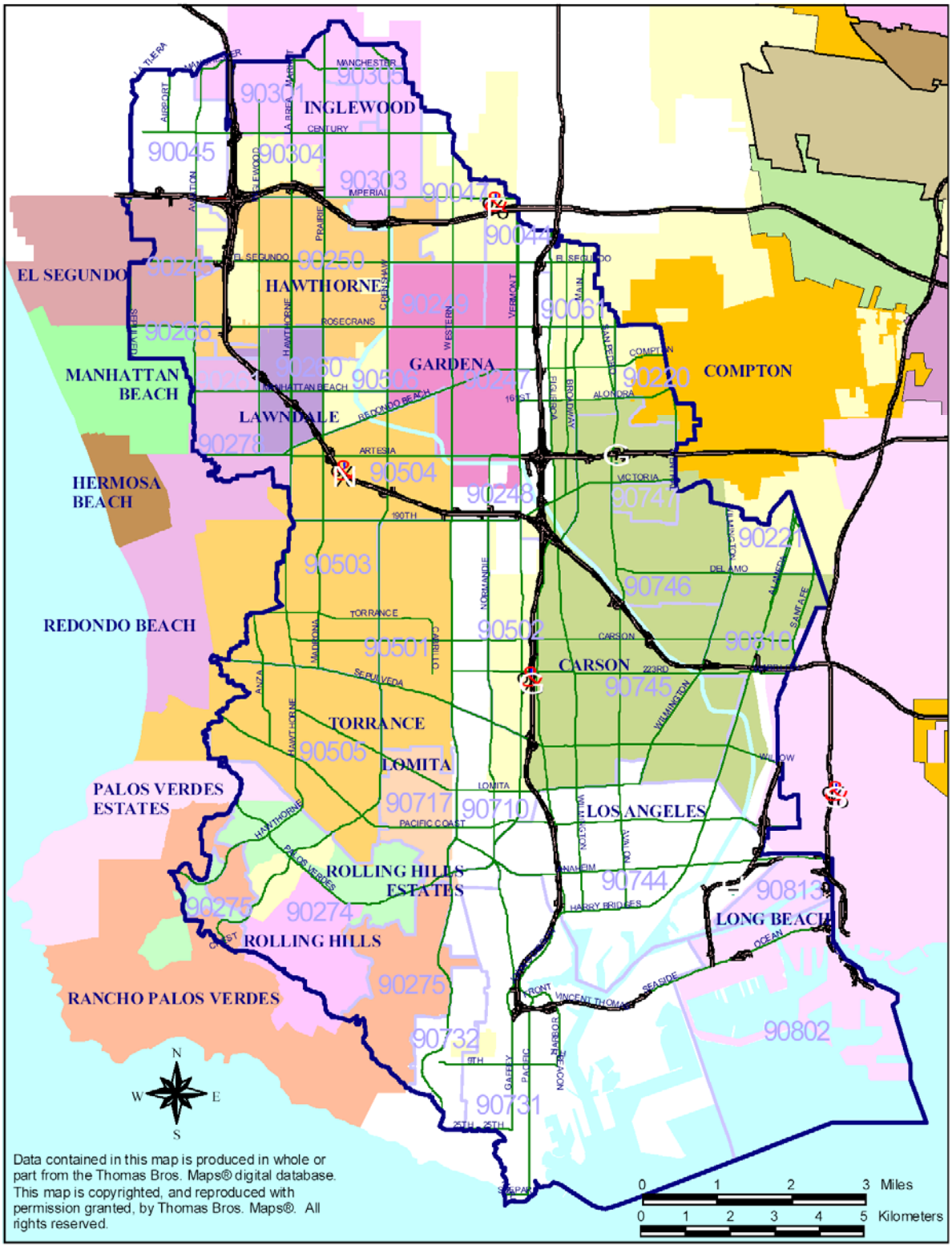

Figure A.2: Cities and zip codes within the Dominguez Watershed (*MEC, 2004*).

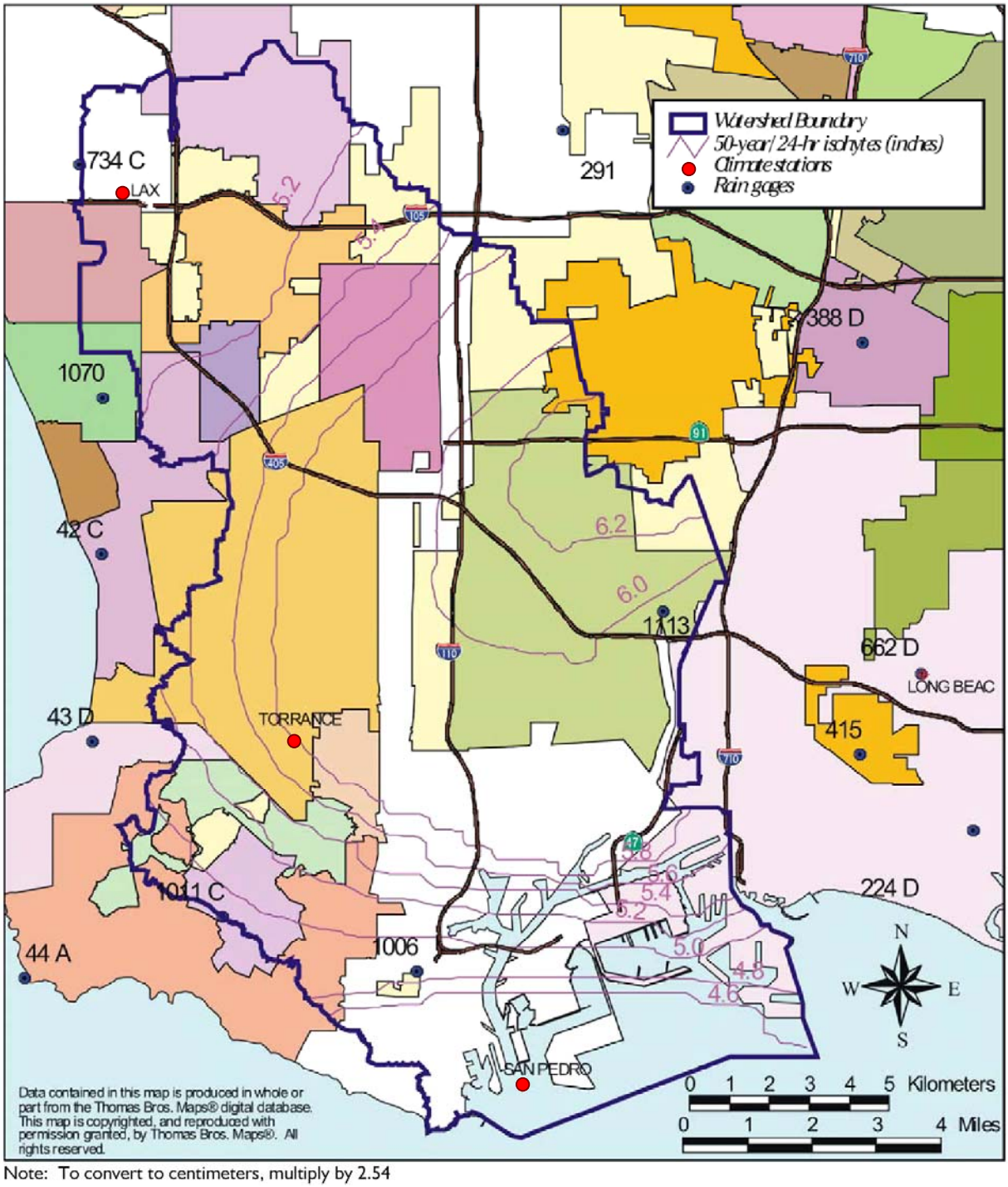

Note: To convert to centimeters, multiply by 2.54

Figure A.3: Isohyetal Map of precipitation (associated with a 50-year, 24-hour rainfall design storm) for the Dominguez Channel Watershed with locations of weather gages (*MEC, 2004*).

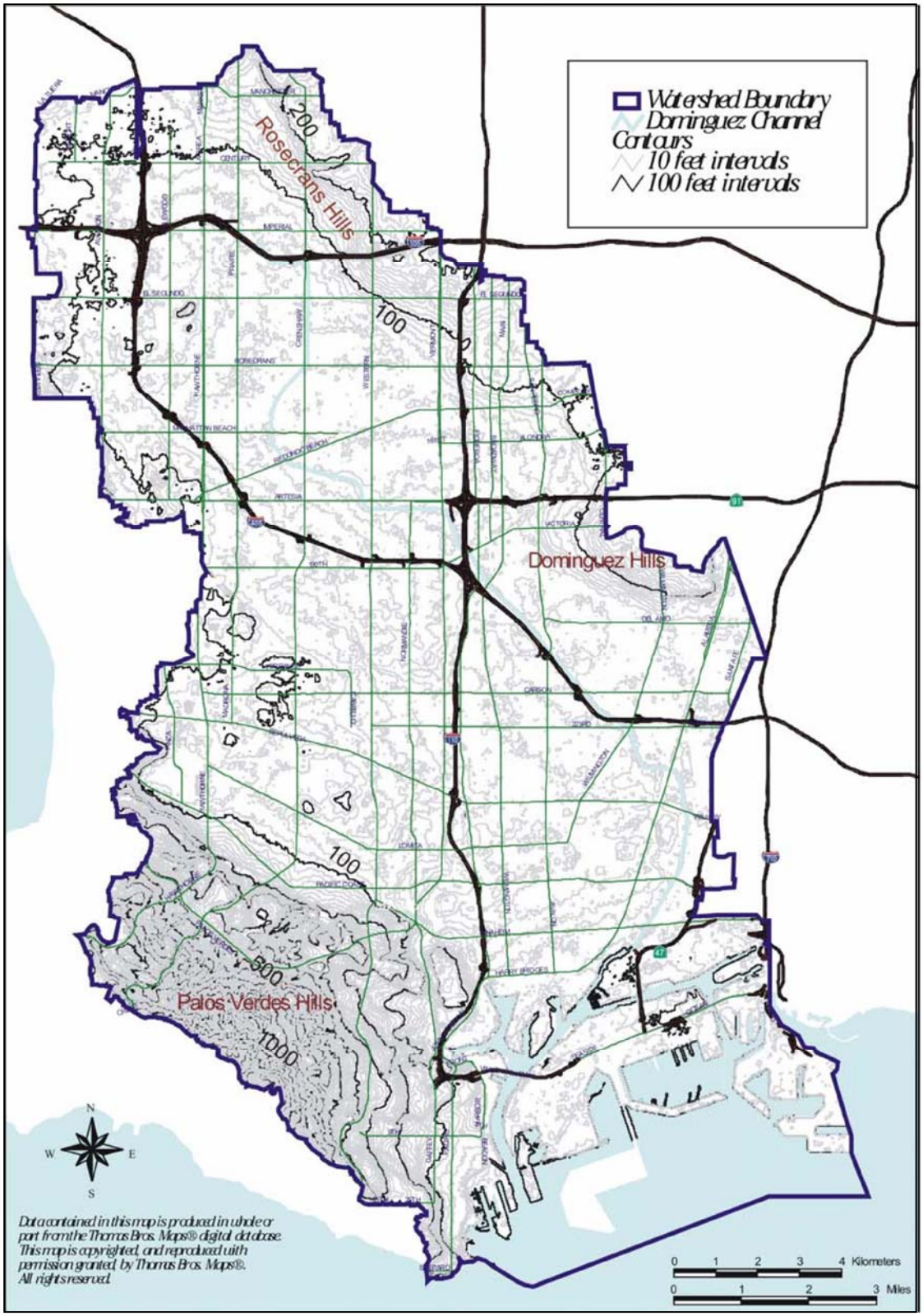

Figure A.4: Dominguez Channel Watershed topography (*MEC, 2004*).

APPENDIX B: Calibration Runs

Table B.1: Record of calibration runs and mass balance calculations

RUN NAME	run1	run2	run3	run4	run5
Rainfall Data	Radar Data	Radar Data	Radar Data	Radar Data	Radar Data
Taken From Run	-	-	-	-	-
Vertical Grid Size (dz), m	dz=0.1	dz=0.1	dz=0.1	dz=0.1	dz=0.1
Specific Storage (Ss), m^{-1}	Ss=1.0E-4	Ss=1.0E-4	Ss=1.0E-4	Ss=1.0E-4	Ss=1.0E-4
Change in Slopes (if any)	-	-	-	-	-
Channel Ksat * (m/hr)	K_chann=0.0001	K_chann=0.0001	K_chann=0.00001	K_chann=0.00001	K_chann=0.0001
Field Ksat (m/hr)	K_field=0.1	K_field=0.1	K_field=0.0001	K_field=0.001	K_field=0.001
Subsurface Ksat (m/hr)					
Channel Porosity	por_chann=0.0001	por_chann=0.0001	por_chann=0.0001	por_chann=0.0001	por_chann=0.0001
Field Porosity	por_field=0.1	por_field=0.1	por_field=0.001	por_field=0.01	por_field=0.001
Subsurface Porosity					
Channel Manning's Coefficient ($hr/m^{1/3}$)	n_chann=1.0E-6	n_chann=7.0E-7	n_chann=7.0E-7	n_chann=1.0E-7	n_chann=1.0E-6
Field Manning's Coefficient ($hr/m^{1/3}$)	n_field=1.0E-5	n_field=1.0E-6	n_field=1.0E-6	n_field=1.0E-6	n_field=1.0E-5
Simulation Time Step	dt=5mins	dt=5mins	dt=5mins	dt=5mins	dt=5mins
Precipitation (P), m^3	4.229E+06	4.229E+06	4.229E+06	4.229E+06	4.229E+06
Runoff (Q) , m^3	2.537E+05	2.585E+05	3.730E+06	2.297E+05	2.297E+05
Compressible Storage (Sc) , m^3	2.777E+03	2.776E+03	4.073E+04	1.634E+04	1.634E+04
Pore Storage (Sp) , m^3	3.929E+06	3.929E+06	2.463E+05	3.927E+06	3.927E+06
Total Subsurface Storage (Sp+Sc) , m^3	3.932E+06	3.932E+06	2.870E+05	3.943E+06	3.943E+06
Surface Storage (ponding) (Ss) , m^3	1.666E+04	1.181E+04	1.716E+05	1.041E+04	1.041E+04
Error (P-Q-Ss-Sp-Sc) , m^3	**2.701E+04**	**2.700E+04**	**4.000E+04**	**4.586E+04**	**4.586E+04**
Error (percent of P)	0.6387	0.6384	0.9458	1.0843	1.0843
Q / P (%)	**5.9979**	**6.1130**	**88.2100**	**5.4313**	**5.4313**

* Ksat: Saturated hydraulic conductivity (m/hour)

Table B.1 (Continued)

run6	run7	run8	run9	run10	run11	run12
Radar Data	Radar Data	Radar Data	Radar Data	Radar Data	Radar Data	Radar Data
-	-	-	-	-	-	-
dz=0.1	dz=0.1	dz=0.1	dz=0.1	dz=0.1	dz=0.1	dz=0.1
Ss=1.0E-4	Ss=1.0E-4	Ss=1.0E-4	Ss=1.0E-4	Ss=1.0E-4	Ss=1.0E-4	Ss=1.0E-4
-	-	Half field slopes	Half field slopes	Half field slopes	Half field slopes	0.9 field slopes
K_chann=0.0001	K_chann=0.0001	K_chann=0.0001	K_chann=0.0001	K_chann=0.0001	K_chann=0.0001	K_chann=0.0001
K_field=0.001	K_field=0.001	K_field=0.001	K_field=0.1	K_field=0.001	K_field=0.001	K_field=0.001
por_chann=0.0001	por_chann=0.0001	por_chann=0.0001	por_chann=0.0001	por_chann=0.0001	por_chann=0.0001	por_chann=0.0001
por_field=0.001	por_field=0.001	por_field=0.001	por_field=0.1	por_field=0.001	por_field=0.001	por_field=0.001
n_chann=3.0E-6	n_chann=1.0E-6	n_chann=1.0E-6	n_chann=1.0E-7	n_chann=5.0E-7	n_chann=5.0E-6	n_chann=1.0E-6
n_field=5.0E-5	n_field=1.0E-5	n_field=1.0E-5	n_field=1.0E-6	n_field=5.0E-6	n_field=5.0E-5	n_field=1.0E-5
dt=5mins	dt=5mins	dt=5mins	dt=5mins	dt=5mins	dt=5mins	dt=5mins
4.229E+06	4.229E+06	4.229E+06	4.229E+06	4.229E+06	4.229E+06	4.229E+06
9.105E+05	2.781E+06	2.449E+06	2.688E+04	3.126E+06	5.812E+05	2.734E+06
4.285E+04	4.250E+04	4.256E+04	2.774E+03	4.243E+04	4.291E+04	4.251E+04
2.463E+05	2.463E+05	2.463E+05	4.099E+04	2.463E+05	2.463E+05	2.463E+05
2.891E+05	2.888E+05	2.888E+05	4.376E+04	2.887E+05	2.892E+05	2.888E+05
2.988E+06	1.117E+06	1.448E+06	1.605E+03	7.723E+05	3.318E+06	1.164E+06
4.178E+04	**4.244E+04**	**4.278E+04**	**4.157E+06**	**4.180E+04**	**4.073E+04**	**4.253E+04**
0.9880	1.0036	1.0116	98.2917	0.9884	0.9631	1.0058
21.5301	**65.7531**	**57.9144**	**0.6356**	**73.9229**	**13.7432**	**64.6370**

Table B.1 (Continued)

run13	run14	run15	run16	run17	run18	run19
Radar Data	Radar Data	Radar Data	Radar Data	Radar Data	Radar Data	Radar Data
-	-	-	-	-	-	-
dz=0.1	dz=0.1	dz=0.1	dz=0.1	dz=0.1	dz=0.1	dz=0.1
Ss=1.0E-4	Ss=1.0E-4	Ss=1.0E-4	Ss=1.0E-4	Ss=1.0E-4	Ss=1.0E-4	Ss=1.0E-4
0.6 field slopes	Half field slopes	Half field slopes	Half field slopes	0.6 field slopes	Half field slopes	Half field slopes
K_chann=0.0001	K_chann=0.0001	K_chann=0.0001	K_chann=0.0001	K_chann=0.0001	K_chann=0.0001	K_chann=0.0001
K_field=0.001	K_field=0.001	K_field=0.001	K_field=0.001	K_field=0.001	K_field=0.001	K_field=0.001
por_chann=0.0001	por_chann=0.0001	por_chann=0.0001	por_chann=0.0001	por_chann=0.0001	por_chann=0.0001	por_chann=0.0001
por_field=0.001	por_field=0.001	por_field=0.001	por_field=0.001	por_field=0.001	por_field=0.001	por_field=0.001
n_chann=1.0E-6	n_chann=5.0E-6	n_chann=1.0E-6	n_chann=1.0E-6	n_chann=1.0E-6	n_chann=9.0E-7	n_chann=1.0E-6
n_field=1.0E-5	n_field=1.0E-5	n_field=5.0E-5	n_field=4.0E-5	n_field=4.0E-5	n_field=4.0E-5	n_field=2.0E-5
dt=5mins	dt=5mins	dt=5mins	dt=5mins	dt=5mins	dt=5mins	dt=5mins
4.229E+06	4.229E+06	4.229E+06	4.229E+06	4.229E+06	4.229E+06	4.229E+06
5.082E+06	2.023E+06	8.320E+05	9.888E+05	1.062E+06	9.998E+05	1.675E+06
4.254E+04	4.265E+04	4.286E+04	4.283E+04	4.282E+04	4.283E+04	4.271E+04
2.463E+05	2.463E+05	2.463E+05	2.463E+05	2.463E+05	2.463E+05	2.463E+05
2.888E+05	2.889E+05	2.891E+05	2.891E+05	2.891E+05	2.891E+05	2.890E+05
1.356E+06	1.873E+06	3.067E+06	2.910E+06	2.836E+06	2.899E+06	2.222E+06
-2.498E+06	**4.379E+04**	**4.085E+04**	**4.144E+04**	**4.162E+04**	**4.144E+04**	**4.284E+04**
-59.0731	1.0356	0.9659	0.9798	0.9842	0.9799	1.0129
120.1703	**47.8340**	**19.6744**	**23.3807**	**25.1194**	**23.6408**	**39.6075**

Table B.1 (Continued)

run20	run21	run21_BC	run22	run23	run24	run25
Radar Data	Radar Data	Radar Data	Radar Data	Radar Data	Radar Data	Radar Data
-	-	-	-	-	-	-
dz=0.1	dz=0.1	dz=0.1	dz=0.1	dz=0.1	dz=0.1	dz=0.1
Ss=1.0E-4	Ss=1.0E-4	Ss=1.0E-4	Ss=1.0E-4	Ss=1.0E-4	Ss=1.0E-4	Ss=1.0E-4
Half field slopes	Half field slopes	Half field slopes	Half field slopes	Half field slopes	Half field slopes	Half field slopes
K_chann=0.0001	K_chann=0.0001	K_chann=0.0001	K_chann=0.0001	K_chann=0.0001	K_chann=0.0001	K_chann=0.0001
K_field=0.01	K_field=0.003	K_field=0.003	K_field=0.03	K_field=0.03	K_field=0.03	K_field=0.03
por_chann=0.0001	por_chann=0.0001	por_chann=0.0001	por_chann=0.0001	por_chann=0.0001	por_chann=0.0001	por_chann=0.0005
por_field=0.01	por_field=0.003	por_field=0.003	por_field=0.003	por_field=0.005	por_field=0.001	por_field=0.001
n_chann=1.0E-6	n_chann=1.0E-6	n_chann=1.0E-6	n_chann=1.0E-6	n_chann=1.0E-6	n_chann=1.0E-6	n_chann=1.0E-6
n_field=2.0E-5	n_field=2.0E-5	n_field=2.0E-5	n_field=2.0E-5	n_field=2.0E-5	n_field=2.0E-5	n_field=2.0E-5
dt=5mins	dt=5mins	dt=5mins	dt=5mins	dt=5mins	dt=5mins	dt=5mins
4.229E+06	4.229E+06	4.229E+06	4.229E+06	4.229E+06	4.229E+06	4.229E+06
4.617E+05	1.329E+06	2.323E+05	1.329E+06	1.021E+06	1.675E+06	1.668E+06
4.251E+04	4.268E+04	9.548E-01	4.268E+04	4.264E+04	4.270E+04	4.270E+04
2.447E+06	7.354E+05	3.345E+05	7.354E+05	1.225E+06	2.463E+05	2.531E+05
2.490E+06	7.780E+05	3.345E+05	7.780E+05	1.267E+06	2.890E+05	2.958E+05
1.238E+06	2.080E+06	9.485E+03	2.080E+06	1.899E+06	2.222E+06	2.222E+06
3.917E+04	**4.218E+04**	**3.653E+06**	**4.216E+04**	**4.136E+04**	**4.282E+04**	**4.286E+04**
0.9261	0.9973	86.3747	0.9968	0.9780	1.0125	1.0134
10.9179	**31.4282**	**5.4921**	**31.4282**	**24.1499**	**39.6075**	**39.4443**

Table B.1 (Continued)

run26	run27	run28	run29	run30	run31	run32
Radar Data	Radar Data	Radar Data	Radar Data	Radar Data	Radar Data	Radar Data
-	-	-	from 28	from 26	from 30	from 31
dz=0.1	dz=0.1	dz=0.1	dz=0.1	dz = 0.2	dz = 0.2	dz = 0.2
Ss=1.0E-4	Ss=2.0E-4	Ss=1.0E-5	Ss=1.0E-5	Ss=1.0E-4	Ss=1.0E-4	Ss=1.0E-4
Half field slopes	Half field slopes	Half field slopes	Half field slopes	Half field slopes	Half field slopes	Half field slopes
K_chann=0.001	K_chann=0.001	K_chann=0.001	K_chann=0.001	K_chann=0.001	K_chann=0.001	K_chann=0.001
K_field=0.03	K_field=0.03	K_field=0.03	K_field=0.03	K_field=0.03	K_field=0.03	K_field=0.03
por_chann=0.0001	por_chann=0.0001	por_chann=0.0001	por_chann=0.0001	por_chann=0.0001	por_chann=0.0001	por_chann=0.0001
por_field=0.001	por_field=0.001	por_field=0.001	por_field=0.001	por_field=0.001	por_field=0.01	por_field=0.01
n_chann=1.0E-6	n_chann=1.0E-6	n_chann=1.0E-6	n_chann=1.0E-6	n_chann=1.0E-6	n_chann=1.0E-6	n_chann=1.0E-7
n_field=2.0E-5	n_field=2.0E-5	n_field=2.0E-5	n_field=2.0E-5	n_field=2.0E-5	n_field=2.0E-5	n_field=2.0E-5
dt=5mins	dt=5mins	dt=5mins	dt=5mins	dt=5mins	dt=5mins	dt=5mins
4.229E+06	4.229E+06	4.229E+06	4.229E+06	4.229E+06	4.229E+06	4.229E+06
1.675E+06	1.632E+06	1.714E+06	1.737E+06	1.334E+06	2.409E+05	2.560E+05
4.270E+04	8.540E+04	4.270E+03	4.271E+03	1.699E+05	5.625E+04	5.624E+04
2.463E+05	2.463E+05	2.463E+05	2.155E+05	5.622E+05	3.852E+06	3.852E+06
2.890E+05	3.317E+05	2.506E+05	2.198E+05	7.321E+05	3.908E+06	3.908E+06
2.222E+06	2.208E+06	2.234E+06	2.242E+06	2.088E+06	1.665E+04	1.597E+03
4.282E+04	**5.722E+04**	**3.005E+04**	**3.043E+04**	**7.503E+04**	**6.321E+04**	**6.314E+04**
1.0125	1.3531	0.7106	0.7195	1.7742	1.4947	1.4930
39.6075	**38.5883**	**40.5297**	**41.0688**	**31.5394**	**5.6961**	**6.0539**

Table B.1 (Continued)

run33	run34	run35	run36	run37	run38	run39
Radar Data	Radar Data	Radar Data	Radar Data	Radar Data	Radar Data	Radar Data
from 32	SUBSURFACE ADDED	from 34	from 34	from 34	from 36	from 38
dz = 0.2	dz = 0.2	dz = 0.1	dz = 0.2	dz = 0.2	dz = 0.2	dz = 0.2
Ss=1.0E-4	Ss=1.0E-4	Ss=1.0E-4	Ss=1.0E-4	Ss=1.0E-4	Ss=1.0E-4	Ss=1.0E-4
Half field slopes	Half field slopes	Half field slopes	Half field slopes	Half field slopes	Half field slopes	0.1 field & channel slopes
K_chann=0.001	K_chann=0.0001	K_chann=0.0001	K_chann=0.0001	K_chann=0.0001	K_chann=0.0001	K_chann=0.0001
K_field=0.03	K_field=0.009	K_field=0.009	K_field=0.001	K_field=0.0001	K_field=0.001	K_field=0.001
	K_subsurf=0.05	K_subsurf=0.05	K_subsurf=0.05	K_subsurf=0.05	K_subsurf=0.1	K_subsurf=0.1
por_chann=0.0001	por_chann=0.0001	por_chann=0.0001	por_chann=0.0001	por_chann=0.0001	por_chann=0.0001	por_chann=0.0001
por_field=0.01	por_field=0.001	por_field=0.001	por_field=0.001	por_field=0.001	por_field=0.005	por_field=0.005
	por_subsurf=0.01	por_subsurf=0.01	por_subsurf=0.01	por_subsurf=0.01	por_subsurf=0.01	por_subsurf=0.01
n_chann=1.0E-7	n_chann=1.0E-7	n_chann=1.0E-7	n_chann=1.0E-7	n_chann=1.0E-7	n_chann=1.0E-7	n_chann=1.0E-7
n_field=6.0E-5	n_field=2.0E-5	n_field=2.0E-5	n_field=2.0E-5	n_field=2.0E-5	n_field=2.0E-5	n_field=2.0E-5
dt=5mins	dt=5mins	dt=5mins	dt=5mins	dt=5mins	dt=5mins	dt=5mins
4.229E+06	4.229E+06	4.229E+06	4.229E+06	4.229E+06	4.229E+06	4.229E+06
2.560E+05	1.522E+05	4.370E+05	1.525E+05	7.898E+05	1.446E+05	1.390E+05
5.624E+04	5.409E+04	4.251E+04	5.379E+04	1.432E+03	5.486E+04	5.492E+04
3.852E+06	3.961E+06	2.607E+06	3.960E+06	2.589E+06	3.967E+06	3.973E+06
3.908E+06	4.015E+06	2.649E+06	4.014E+06	2.591E+06	4.022E+06	4.028E+06
1.597E+03	0.000E+00	1.241E+06	0.000E+00	7.904E+05	0.000E+00	0.000E+00
6.314E+04	**6.218E+04**	**-9.746E+04**	**6.237E+04**	**5.826E+04**	**6.230E+04**	**6.230E+04**
1.4930	1.4703	-2.3047	1.4747	1.3776	1.4732	1.4731
6.0539	**3.5997**	**10.3322**	**3.6070**	**18.6753**	**3.4202**	**3.2864**

Table B.1 (Continued)

run40	run41	run42	run43	run44	run45
Radar Data from 39 dz = 0.2 Ss=1.0E-4 0.1 field & channel slopes	Radar Data from 39 dz = 0.2 Ss=1.0E-4 0.1 field & channel slopes	Radar Data from 39 dz = 0.2 Ss=1.0E-4 0.1 field & channel slopes	Radar Data from 40 dz = 0.2 Ss=1.0E-4 0.1 field & channel slopes	Radar Data from 42 dz = 0.2 Ss=1.0E-4 Half field slopes	Radar Data from 37 dz = 0.2 Ss=1.0E-4 0.25 field slopes
K_chann=0.0001	K_chann=0.0001	K_chann=0.0001	K_chann=0.0001	K_chann=0.0001	K_chann=0.0001
K_field=0.001	K_field=0.001	K_field=0.001	K_field=0.0001	K_field=0.001	K_field=0.0001
K_subsurf=0.1	K_subsurf=0.1	K_subsurf=0.1	K_subsurf=0.1	K_subsurf=0.1	K_subsurf=0.05
por_chann=0.0001	por_chann=0.0001	por_chann=0.0001	por_chann=0.0001	por_chann=0.0001	por_chann=0.0001
por_field=0.005	por_field=0.005	por_field=0.005	por_field=0.005	por_field=0.005	por_field=0.001
por_subsurf=0.01	por_subsurf=0.01	por_subsurf=0.01	por_subsurf=0.01	por_subsurf=0.01	por_subsurf=0.01
n_chann=1.0E-6	n_chann=1.0E-7	n_chann=1.0E-6	n_chann=1.0E-6	n_chann=1.0E-6	n_chann=1.0E-7
n_field=2.0E-5	n_field=1.0E-4	n_field=5.0E-6	n_field=2.0E-5	n_field=5.0E-6	n_field=2.0E-5
dt=5mins	dt=5mins	dt=5mins	dt=5mins	dt=5mins	dt=5mins
4.229E+06	4.229E+06	4.229E+06	4.229E+06	4.229E+06	4.229E+06
9.461E+04	1.390E+05	9.467E+04	9.467E+04	1.203E+05	5.968E+05
5.517E+04	5.492E+04	5.517E+04	5.517E+04	5.508E+04	1.444E+03
4.007E+06	3.973E+06	4.007E+06	4.007E+06	3.991E+06	2.611E+06
4.062E+06	4.028E+06	4.062E+06	4.062E+06	4.046E+06	2.612E+06
1.008E+04	0.000E+00	1.009E+04	1.009E+04	1.112E+02	9.617E+05
6.254E+04	**6.232E+04**	**6.257E+04**	**6.257E+04**	**6.237E+04**	**5.814E+04**
1.4788	1.4736	1.4795	1.4795	1.4749	1.3747
2.2371	**3.2859**	**2.2386**	**2.2386**	**2.8456**	**14.1109**

Table B.1 (Continued)

run46	RainLAX	RainCenter	RainOutlet	run47	run48	run49
Radar Data	LAX Raingage	Center Raingage	Outlet Raingage	Radar Data	Radar Data	Radar Data
from 37	from 46	from 46	from 46	from 46	from 46	from 21 w subsurf
dz = 0.2	dz = 0.2	dz = 0.2	dz = 0.2	dz = 0.2	dz = 0.2	dz = 0.1
Ss=1.0E-4	Ss=1.0E-4	Ss=1.0E-4	Ss=1.0E-4	Ss=1.0E-4	Ss=1.0E-4	Ss=1.0E-4
0.05 field slopes	0.05 field slopes	0.05 field slopes	0.05 field slopes	0.05 field slopes	0.05 field slopes	Half field slopes
K_chann=0.0001	K_chann=0.0001	K_chann=0.0001	K_chann=0.0001	K_chann=0.0001	K_chann=0.0001	K_chann=0.0001
K_field=0.0001	K_field=0.0001	K_field=0.0001	K_field=0.0001	K_field=0.0005	K_field=0.00005	K_field=0.003
K_subsurf=0.05	K_subsurf=0.05	K_subsurf=0.05	K_subsurf=0.05	K_subsurf=1	K_subsurf=1	K_subsurf=0.05
por_chann=0.0001	por_chann=0.0001	por_chann=0.0001	por_chann=0.0001	por_chann=0.0001	por_chann=0.0001	por_chann=0.0001
por_field=0.001	por_field=0.001	por_field=0.001	por_field=0.001	por_field=0.001	por_field=0.001	por_field=0.003
por_subsurf=0.01	por_subsurf=0.01	por_subsurf=0.01	por_subsurf=0.01	por_subsurf=0.3	por_subsurf=0.3	por_subsurf=0.01
n_chann=1.0E-7	n_chann=1.0E-7	n_chann=1.0E-7	n_chann=1.0E-7	n_chann=1.0E-7	n_chann=1.0E-7	n_chann=1.0E-6
n_field=2.0E-5	n_field=2.0E-5	n_field=2.0E-5	n_field=2.0E-5	n_field=2.0E-5	n_field=2.0E-5	n_field=2.0E-5
dt=5mins	dt=5mins	dt=5mins	dt=5mins	dt=5mins	dt=5mins	dt=5mins
4.229E+06	5.817E+06	4.514E+06	4.229E+06	4.229E+06	4.229E+06	4.229E+06
2.083E+05	4.224E+05	2.332E+05	2.083E+05	5.427E+05	5.427E+05	3.383E+05
1.464E+03	5.406E+02	1.638E+03	1.464E+03	0.000E+00	0.000E+00	4.253E+04
2.636E+06	2.527E+06	2.664E+06	2.636E+06	3.919E+04	3.919E+04	2.500E+06
2.637E+06	2.527E+06	2.665E+06	2.637E+06	3.919E+04	3.919E+04	2.543E+06
1.326E+06	2.801E+06	1.556E+06	1.326E+06	3.625E+06	3.625E+06	1.309E+06
5.750E+04	**6.632E+04**	**5.928E+04**	**5.750E+04**	**2.197E+04**	**2.197E+04**	**3.941E+04**
1.3596	1.1401	1.3133	1.3596	0.5195	0.5195	0.9320
4.9265	**7.2619**	**5.1658**	**4.9265**	**12.8338**	**12.8338**	**7.9986**

Table B.1 (Continued)

run50	run51	run52	run53	run54	run55	run57
Radar Data from 21 w subsurf dz = 0.1 Ss=1.0E-4 Half field slopes	Radar Data from 21 w subsurf dz = 0.1 Ss=1.0E-4 Half field slopes	Radar Data from 21 w subsurf dz = 0.1 Ss=1.0E-4 Half field slopes	Radar Data from 21 w subsurf dz = 0.1 Ss=1.0E-4 Half field slopes	Radar Data from 49 dz = 0.1 Ss=1.0E-4 Half field slopes	Radar Data from 49 dz = 0.1 Ss=1.0E-4 Half field slopes	Radar Data from 54 dz = 0.1, two cell field Ss=1.0E-4 Half field slopes
K_chann=0.0001	K_chann=0.0001	K_chann=0.0001	K_chann=0.0001	K_chann=0.0001	K_chann=0.0001	K_chann=0.0001
K_field=0.003	K_field=0.003	K_field=0.003	K_field=0.003	K_field=0.001	K_field=0.0005	K_field=0.001
K_subsurf=0.05	K_subsurf=0.05	K_subsurf=0.05	K_subsurf=0.05	K_subsurf=0.05	K_subsurf=0.05	K_subsurf=0.05
por_chann=0.0001	por_chann=0.0001	por_chann=0.0001	por_chann=0.0001	por_chann=0.0001	por_chann=0.0001	por_chann=0.0001
por_field=0.003	por_field=0.003	por_field=0.003	por_field=0.003	por_field=0.003	por_field=0.003	por_field=0.003
por_subsurf=0.01	por_subsurf=0.01	por_subsurf=0.01	por_subsurf=0.01	por_subsurf=0.01	por_subsurf=0.01	por_subsurf=0.01
n_chann=1.0E-7	n_chann=1.0E-6	n_chann=1.0E-6	n_chann=1.0E-6	n_chann=1.0E-6	n_chann=1.0E-6	n_chann=1.0E-6
n_field=2.0E-5	n_field=1.0E-6	n_field=5.0E-6	n_field=4.0E-6	n_field=4.0E-6	n_field=4.0E-6	n_field=4.0E-6
dt=5mins	dt=5mins	dt=5mins	dt=5mins	dt=5mins	dt=5mins	dt=5mins
4.229E+06	4.229E+06	4.229E+06	4.229E+06	4.229E+06	4.229E+06	4.229E+06
4.245E+05	1.405E+06	9.150E+05	1.011E+06	1.011E+06	1.011E+06	1.205E+06
4.275E+04	4.257E+04	4.266E+04	4.264E+04	4.264E+04	4.264E+04	3.976E+04
2.514E+06	2.514E+06	2.514E+06	2.514E+06	2.514E+06	2.514E+06	2.304E+06
2.557E+06	2.556E+06	2.557E+06	2.557E+06	2.557E+06	2.557E+06	2.344E+06
1.232E+06	2.516E+05	7.403E+05	6.445E+05	6.445E+05	6.445E+05	6.401E+05
1.594E+04	**1.619E+04**	**1.708E+04**	**1.700E+04**	**1.701E+04**	**1.701E+04**	**4.013E+04**
0.3769	0.3827	0.4039	0.4020	0.4022	0.4022	0.9489
10.0381	**33.2183**	**21.6373**	**23.9064**	**23.9064**	**23.9064**	**28.4914**

Table B.1 (Continued)

run58	run59	run60	run61	run62	run63	run64
Radar Data from 57	Radar Data from 57	Radar Data from 57	Radar Data from 60	Radar Data from 61	Radar Data from 62	Radar Data from 63
dz = 0.1, two cell field	dz = 0.1, two cell field	dz = 0.1, two cell field	dz = 0.1, two cell field	dz = 0.1, 3 cell field	dz = 0.1, 3 cell field	dz = 0.1, 3 cell field
Ss=1.0E-4	Ss=1.0E-4	Ss=1.0E-4	Ss=1.0E-4	Ss=1.0E-4	Ss=1.0E-4	Ss=1.0E-4
Half field slopes	Half field slopes	Half field slopes	Half field slopes	Half field slopes	Half field slopes	Half field slopes
K_chann=0.0001	K_chann=0.0001	K_chann=0.0001	K_chann=0.0001	K_chann=0.0001	K_chann=0.0001	K_chann=0.0001
K_field=0.001	K_field=0.001	K_field=0.001	K_field=0.001	K_field=0.001	K_field=0.001	K_field=0.001
K_subsurf=0.05	K_subsurf=0.05	K_subsurf=0.05	K_subsurf=0.05	K_subsurf=0.05	K_subsurf=0.05	K_subsurf=0.05
por_chann=0.0001	por_chann=0.0001	por_chann=0.0001	por_chann=0.0001	por_chann=0.0001	por_chann=0.0001	por_chann=0.0001
por_field=0.003	por_field=0.003	por_field=0.003	por_field=0.003	por_field=0.003	por_field=0.003	por_field=0.003
por_subsurf=0.01	por_subsurf=0.2	por_subsurf=0.1	por_subsurf=0.1	por_subsurf=0.1	por_subsurf=0.1	por_subsurf=0.1
n_chann=1.0E-7	n_chann=1.0E-7	n_chann=5.0E-7	n_chann=2.0E-7	n_chann=2.0E-7	n_chann=5.0E-7	n_chann=1.0E-7
n_field=2.0E-6	n_field=2.0E-6	n_field=2.0E-6	n_field=2.0E-6	n_field=2.0E-6	n_field=2.0E-6	n_field=2.0E-6
dt=5mins	dt=5mins	dt=5mins	dt=5mins	dt=5mins	dt=5mins	dt=5mins
4.229E+06	4.229E+06	4.229E+06	4.229E+06	4.229E+06	4.229E+06	4.229E+06
1.564E+06	2.968E+05	3.050E+05	3.091E+05	5.593E+05	5.543E+05	5.608E+05
3.970E+04	0.000E+00	0.000E+00	0.000E+00	0.000E+00	0.000E+00	0.000E+00
2.302E+06	3.909E+06	3.897E+06	3.893E+06	3.643E+06	3.645E+06	3.641E+06
2.342E+06	3.909E+06	3.897E+06	3.893E+06	3.643E+06	3.645E+06	3.641E+06
2.837E+05	0.000E+00	7.349E+02	0.000E+00	2.014E+02	3.089E+03	0.000E+00
3.916E+04	**2.285E+04**	**2.666E+04**	**2.663E+04**	**2.691E+04**	**2.695E+04**	**2.698E+04**
0.9259	0.5403	0.6303	0.6297	0.6363	0.6373	0.6380
36.9827	**7.0170**	**7.2123**	**7.3083**	**13.2251**	**13.1062**	**13.2613**

Table B.1 (Continued)

run65	run66	run67	run68	run69	run70	run71
Radar Data from 57	Radar Data from 65	Radar Data from 66	Radar Data from 65	Radar Data from 67	Radar Data from 69	Radar Data from 70
dz = 0.1, 3 cell field	dz = 0.1, 3 cell field	dz = 0.1, 3 cell field	dz = 0.1, 3 cell field	dz = 0.1, 3 cell field	dz = 0.1, 3 cell field	dz = 0.1, 3 cell field
Ss=1.0E-4	Ss=1.0E-4	Ss=1.0E-4	Ss=1.0E-4	Ss=1.0E-4	Ss=1.0E-4	Ss=1.0E-4
Half field slopes	Half field slopes	Half field slopes	Half field slopes	Half field slopes	Half field slopes	Half field slopes
K_chann=0.0001	K_chann=0.0001	K_chann=0.0001	K_chann=0.0001	K_chann=0.0001	K_chann=0.0001	K_chann=0.0001
K_field=0.001	K_field=0.001	K_field=0.001	K_field=0.001	K_field=0.001	K_field=0.001	K_field=0.001
K_subsurf=0.05	K_subsurf=0.05	K_subsurf=0.05	K_subsurf=0.05	K_subsurf=0.05	K_subsurf=0.05	K_subsurf=0.05
por_chann=0.0001	por_chann=0.0001	por_chann=0.0001	por_chann=0.0001	por_chann=0.0001	por_chann=0.00009	por_chann=0.00009
por_field=0.003	por_field=0.003	por_field=0.003	por_field=0.003	por_field=0.003	por_field=0.003	por_field=0.003
por_subsurf=0.01	por_subsurf=0.01	por_subsurf=0.01	por_subsurf=0.01	por_subsurf=0.01	por_subsurf=0.01	por_subsurf=0.01
n_chann=1.0E-6	n_chann=1.0E-7	n_chann=1.0E-7	n_chann=5.0E-7	n_chann=1.0E-7	n_chann=1.0E-7	n_chann=3.0E-7
n_field=4.0E-6	n_field=4.0E-6	n_field=5.0E-6	n_field=4.0E-6	n_field=6.0E-6	n_field=6.0E-6	n_field=6.0E-6
dt=5mins	dt=5mins	dt=5mins	dt=5mins	dt=5mins	dt=5mins	dt=5mins
4.229E+06	4.229E+06	4.229E+06	4.229E+06	4.229E+06	4.229E+06	4.229E+06
1.327E+06	1.452E+06	1.351E+06	1.386E+06	1.262E+06	1.262E+06	1.223E+06
3.964E+04	3.964E+04	3.965E+04	3.964E+04	3.967E+04	3.967E+04	3.967E+04
2.176E+06	2.174E+06	2.174E+06	2.175E+06	2.174E+06	2.174E+06	2.175E+06
2.215E+06	2.214E+06	2.214E+06	2.215E+06	2.214E+06	2.214E+06	2.214E+06
6.464E+05	5.234E+05	6.240E+05	5.884E+05	7.131E+05	7.131E+05	7.520E+05
4.021E+04	**3.970E+04**	**3.991E+04**	**3.997E+04**	**3.994E+04**	**3.994E+04**	**3.998E+04**
0.9508	0.9386	0.9436	0.9452	0.9444	0.9444	0.9453
31.3809	**34.3391**	**31.9555**	**32.7737**	**29.8487**	**29.8487**	**28.9170**

Table B.1 (Continued)

run72	run73_LAX	run74_center	run75_outlet	run76_LAX	run77_LAX
Radar Data from 70	LAX Raingage from 72	Center Raingage from 72	Outlet Raingage from 72	LAX Raingage from 73_LAX	LAX Raingage from 73_LAX
dz = 0.1, 3 cell field	dz = 0.1, 3 cell field	dz = 0.1, 3 cell field	dz = 0.1, 3 cell field	dz = 0.1, 3 cell field	dz = 0.1, 3 cell field
Ss=1.0E-4	Ss=1.0E-4	Ss=1.0E-4	Ss=1.0E-4	Ss=1.0E-4	Ss=1.0E-4
Half field slopes	Half field slopes	Half field slopes	Half field slopes	Half field slopes	Half field slopes
K_chann=0.0001	K_chann=0.0001	K_chann=0.0001	K_chann=0.0001	K_chann=0.0001	K_chann=0.0001
K_field=0.001	K_field=0.001	K_field=0.001	K_field=0.001	K_field=0.001	K_field=0.001
K_subsurf=0.05	K_subsurf=0.05	K_subsurf=0.05	K_subsurf=0.05	K_subsurf=0.05	K_subsurf=0.05
por_chann=0.00009	por_chann=0.00009	por_chann=0.00009	por_chann=0.00009	por_chann=0.00009	por_chann=0.00009
por_field=0.003	por_field=0.003	por_field=0.003	por_field=0.003	por_field=0.003	por_field=0.003
por_subsurf=0.01	por_subsurf=0.01	por_subsurf=0.01	por_subsurf=0.01	por_subsurf=0.01	por_subsurf=0.01
n_chann=2.0E-7	n_chann=2.0E-7	n_chann=2.0E-7	n_chann=2.0E-7	n_chann=2.0E-7	n_chann=2.0E-7
n_field=6.0E-6	n_field=6.0E-6	n_field=6.0E-6	n_field=6.0E-6	n_field=7.0E-6	n_field=1.0E-5
dt=5mins	dt=5mins	dt=5mins	dt=5mins	dt=5mins	dt=5mins
4.229E+06	5.817E+06	4.514E+06	3.443E+06	5.817E+06	5.817E+06
1.241E+06	2.432E+06	1.408E+06	6.692E+05	2.301E+06	1.978E+06
3.967E+04	3.973E+04	3.969E+04	3.963E+04	3.975E+04	3.981E+04
2.174E+06	2.171E+06	2.174E+06	2.174E+06	2.171E+06	2.171E+06
2.214E+06	2.211E+06	2.214E+06	2.214E+06	2.211E+06	2.211E+06
7.344E+05	1.123E+06	8.496E+05	5.255E+05	1.254E+06	1.577E+06
3.994E+04	**5.157E+04**	**4.215E+04**	**3.455E+04**	**5.165E+04**	**5.169E+04**
0.9444	0.8866	0.9337	1.0034	0.8879	0.8885
29.3379	**41.8053**	**31.1948**	**19.4377**	**39.5603**	**34.0061**

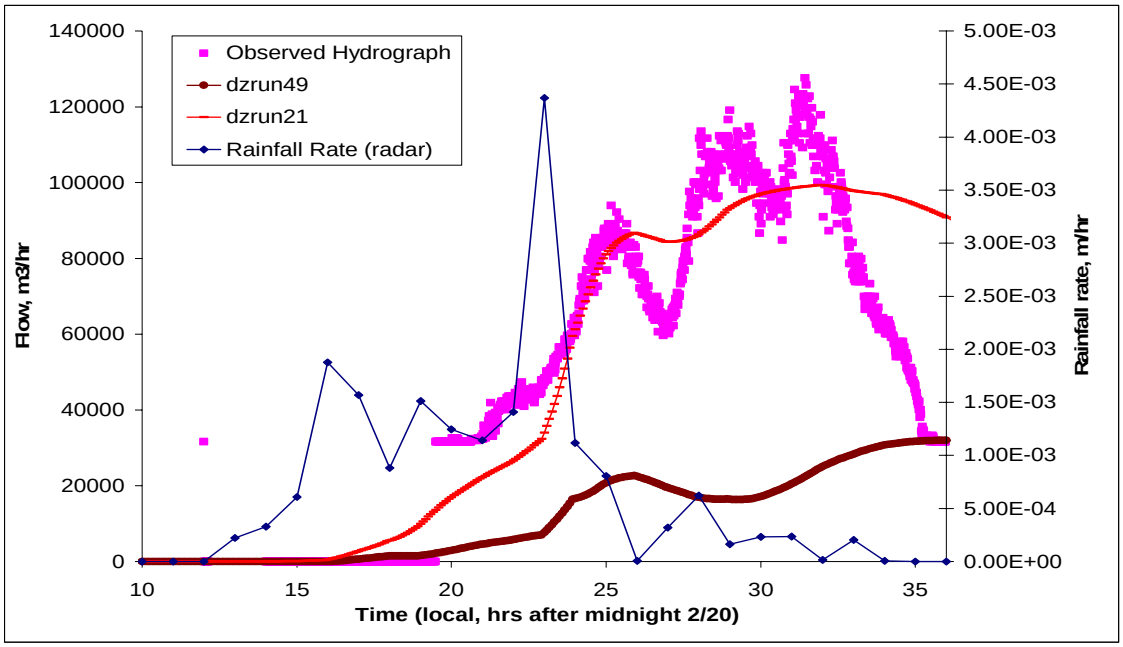

Figure B.1: Comparison of runs with (run49) or without (run21) a subsurface layer assigned.

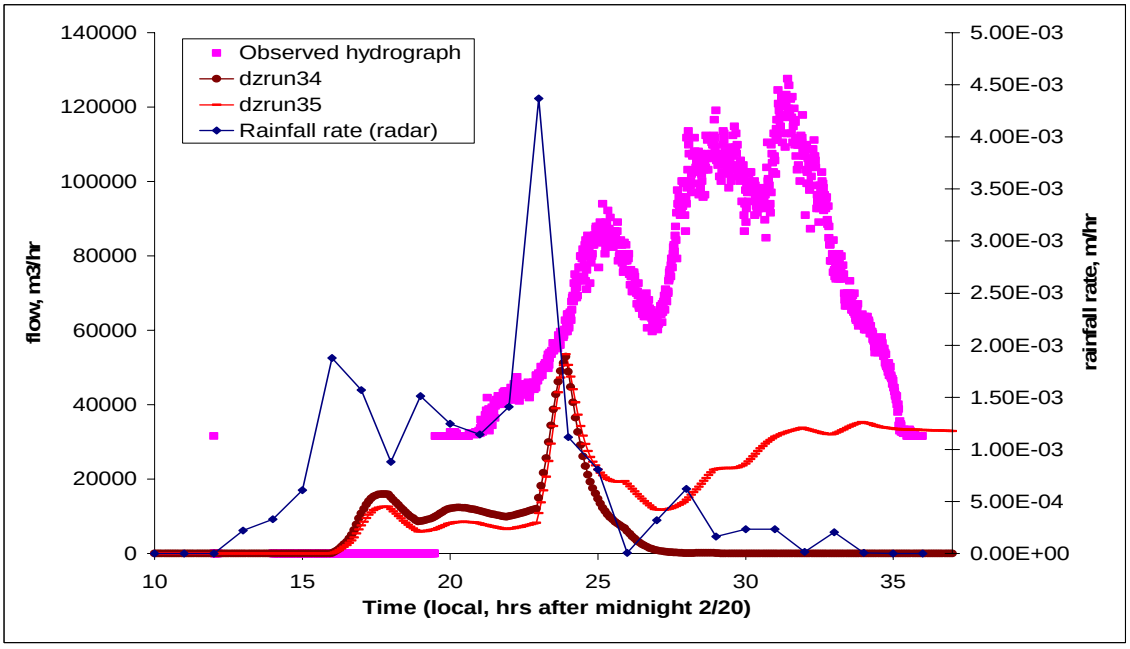

Figure B.2: Comparison of runs with different vertical cell size;
run34 (dz=0.2) and run35 (dz=0.1)

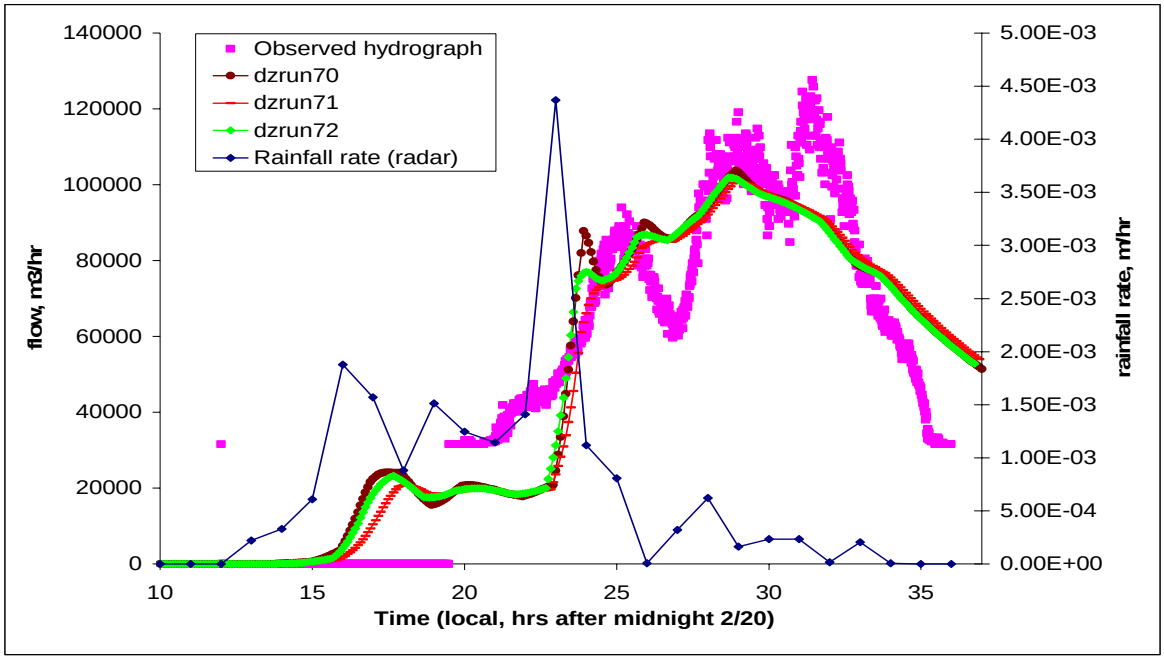

Figure B.3: Comparison of runs with different channel Manning's Coefficient; run70 (1.0E-7), run72 (2.0E-7), and run71 (3.0E-7).

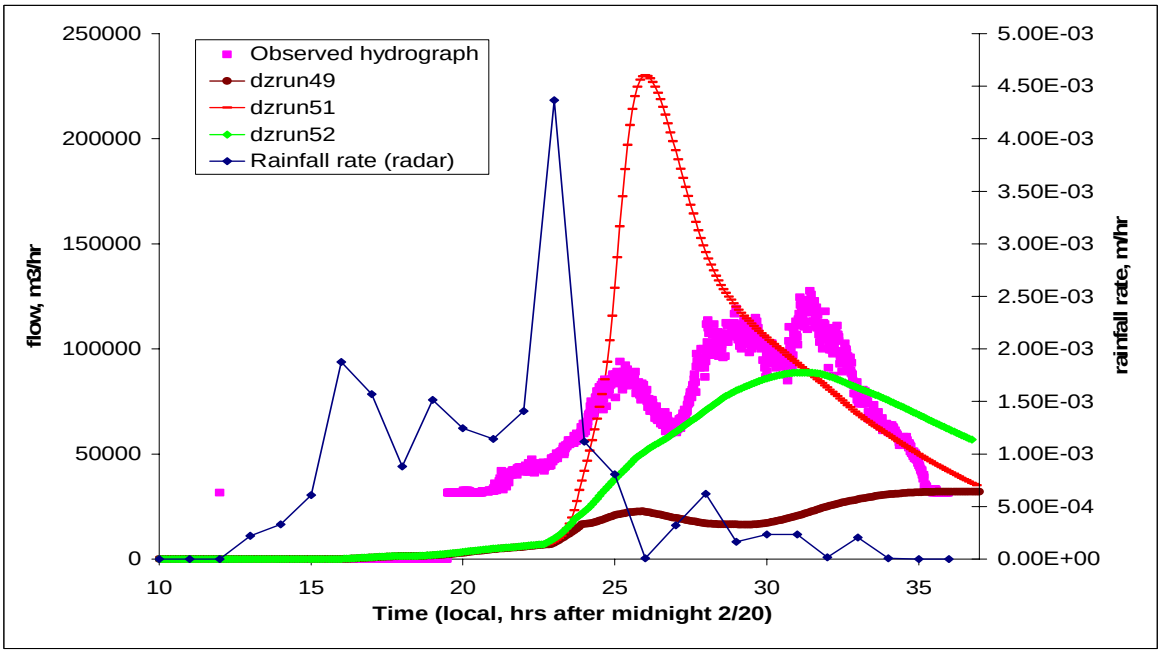

Figure B.4: Comparison of runs with different field Manning's Coefficient; run51 (1.0E-6), run52 (5.0E-6), and run49 (2.0E-5).

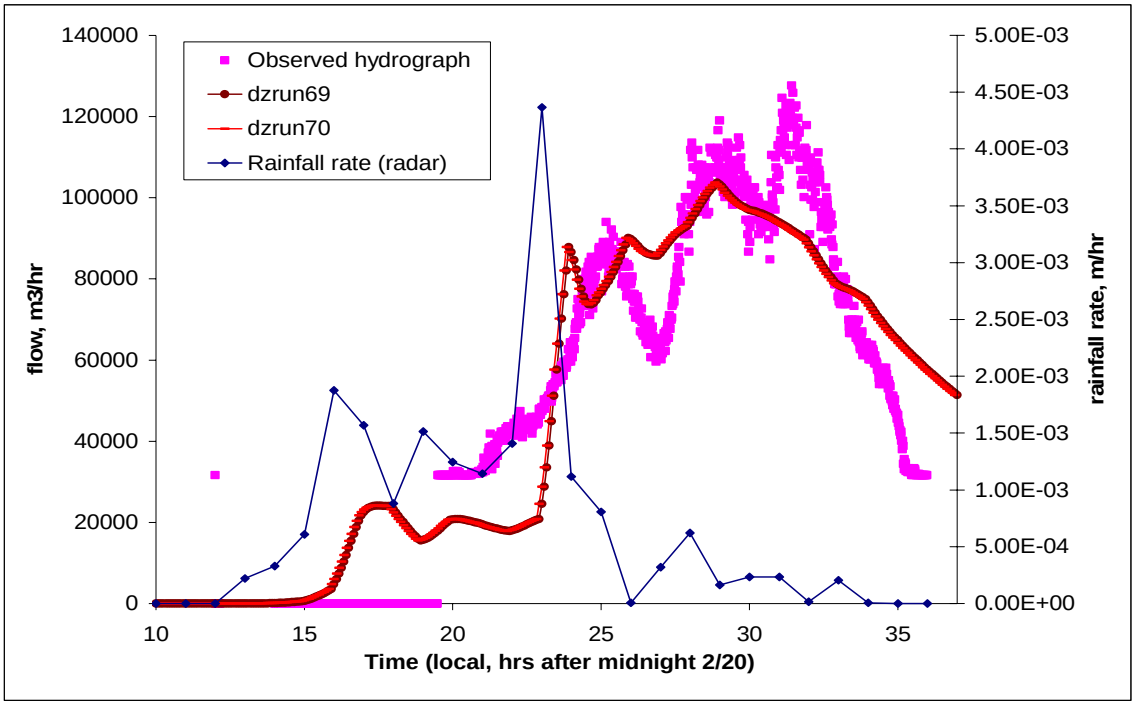

Figure B.5: Comparison of runs with different channel porosity; run70 (0.00009) and run69 (0.0001)

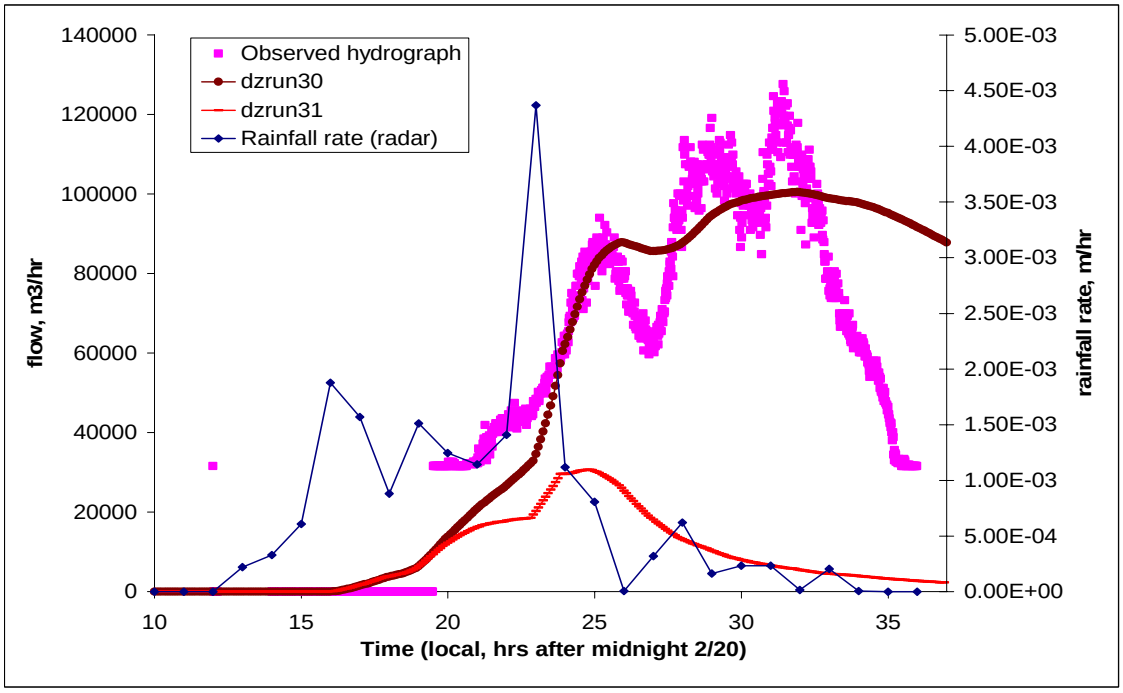

Figure B.6: Comparison of runs with different field porosity; Run30 (0.001) and run21 (0.01)

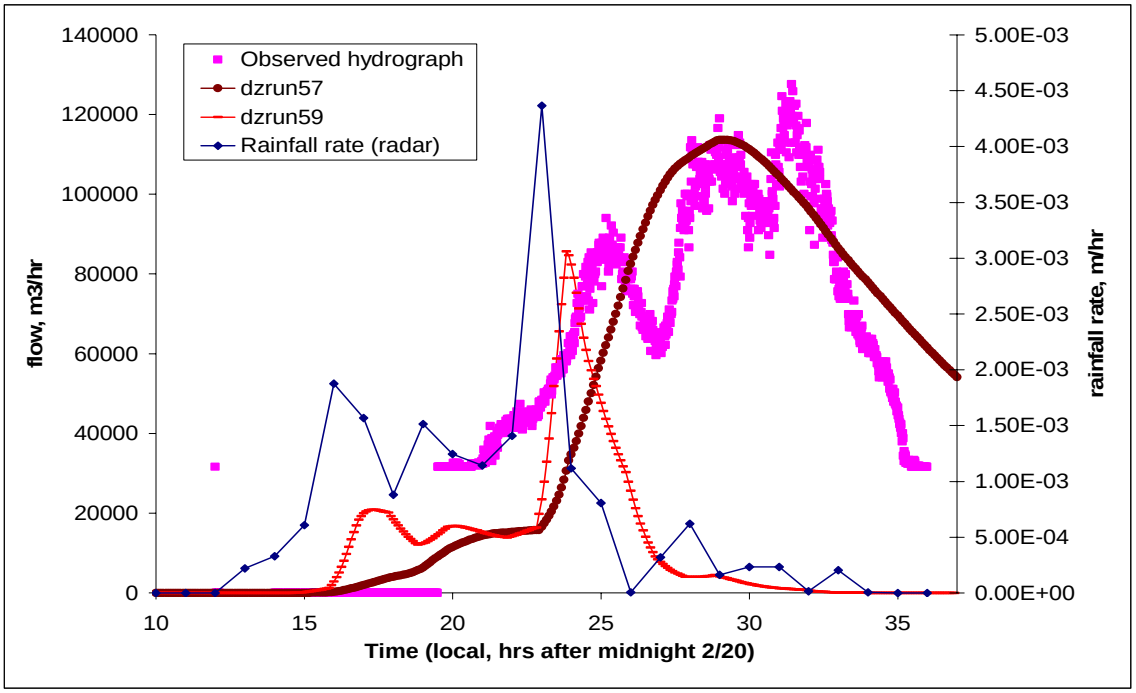

Figure B.7: Comparison of runs with different subsurface porosity; Run57 (0.01) and run59 (0.2)

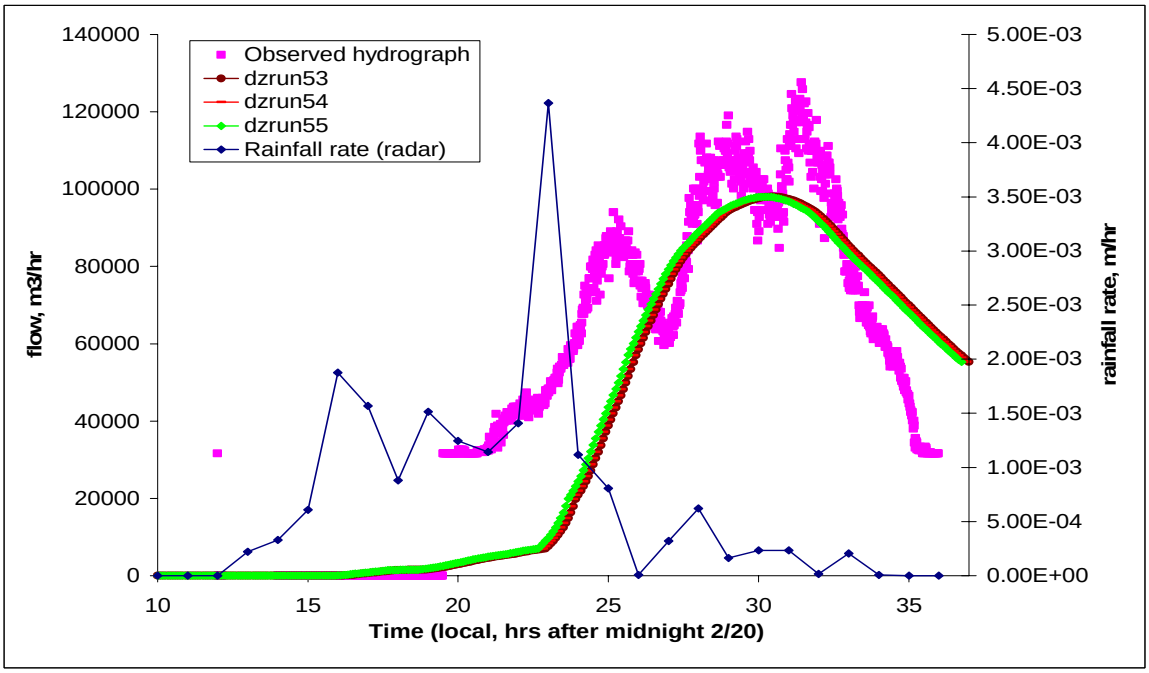

Figure B.8: Comparison of runs with different field hydraulic conductivity; Run55 (0.0005), run54 (0.001), and run53 (0.003)

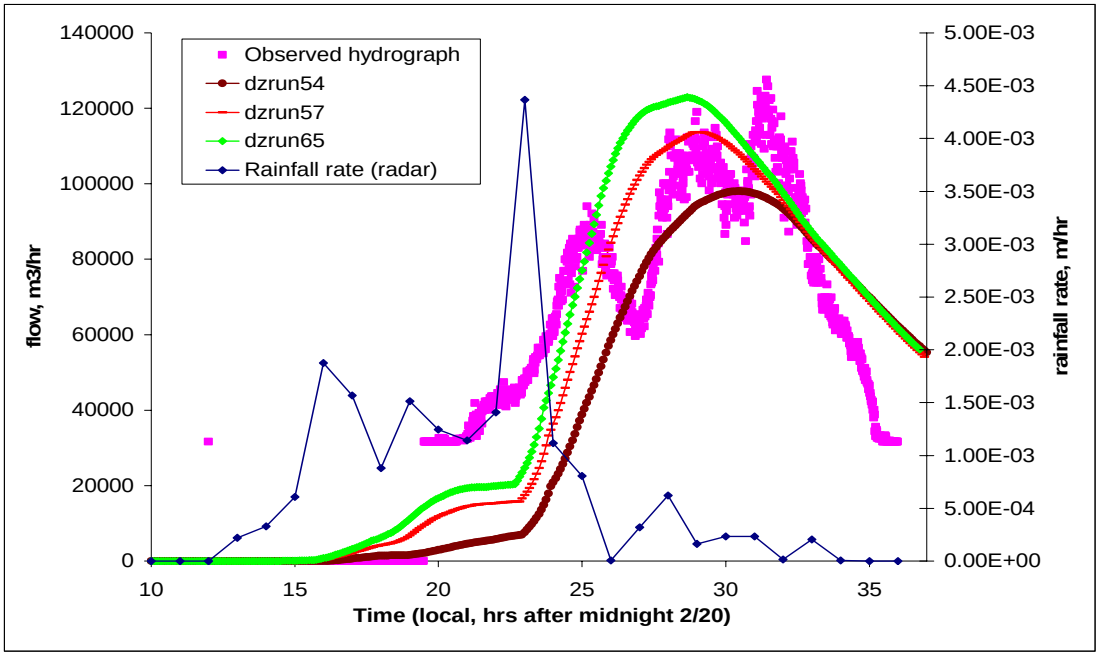

Figure B.9: Comparison of runs with different surface layer thickness; Run54 (1 layer), run57 (2 layers), and run65 (3 layers)

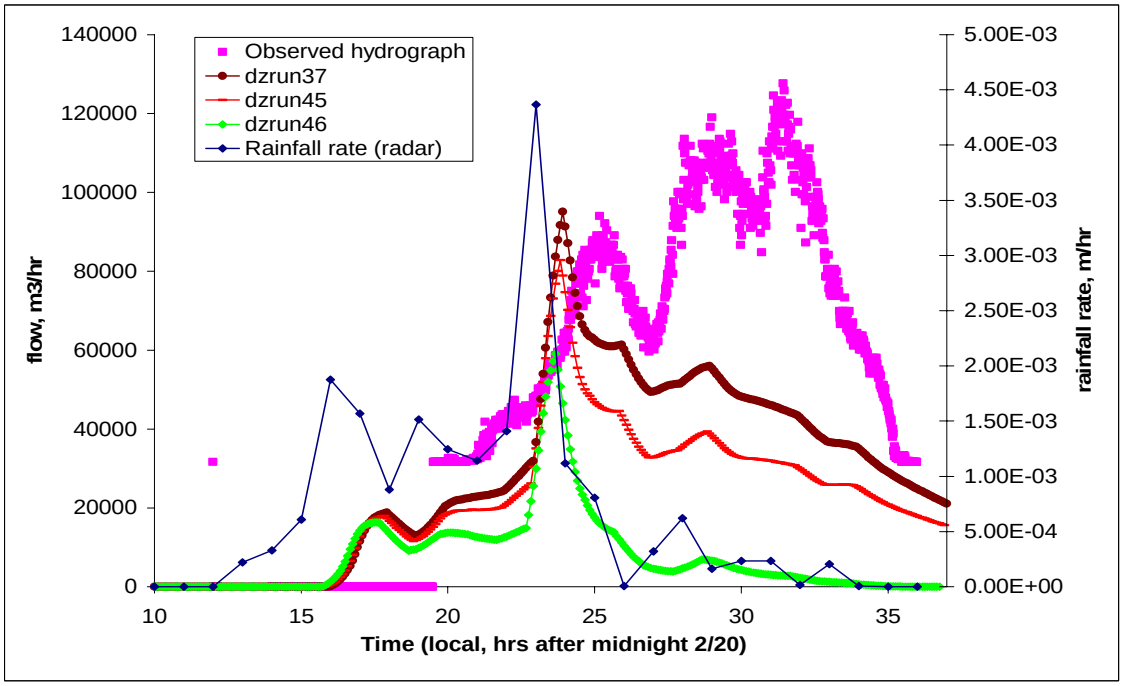

Figure B.10: Comparison of runs with different field slopes; Run37 (0.5*processed field slopes), run45 (0.25*processed field slopes), and run46 (0.05*processed field slopes).